Recipes for How to Force Oceanic Model Dynamics

Lionel Renault, Sébastien Masson, Thomas Arsouze, Gurvan Madec, James C. Mcwilliams

JAMES | Journal of Advances in Modeling Earth Systems

RESEARCH ARTICLE
10.1029/2019MS001715

Recipes for How to Force Oceanic Model Dynamics

Lionel Renault[1,2], S. Masson[3], T. Arsouze[4], Gurvan Madec[3], and James C. McWilliams[2]

[1]LEGOS, University of Toulouse, IRD, CNRS, CNES, UPS, Toulouse, France, [2]Department of Atmospheric and Oceanic Sciences, University of California, Los Angeles, CA, USA, [3]Sorbonne Universites (UPMC Univ Paris 06)-CNRS-IRD-MNHN, Paris, France, [4]Barcelona Super Computing Center, Barcelona, Spain

Abstract The current feedback to the atmosphere (CFB) contributes to the oceanic circulation by damping eddies. In an ocean-atmosphere coupled model, CFB can be correctly accounted for by using the wind relative to the oceanic current. However, its implementation in a forced oceanic model is less straightforward as CFB also enhances the 10-m wind. Wind products based on observations have seen real currents that will not necessarily correspond to model currents, whereas meteorological reanalyses often neglect surface currents or use surface currents that, again, will differ from the surface currents of the forced oceanic simulation. In this study, we use a set of quasi-global oceanic simulations, coupled or not with the atmosphere, to (i) quantify the error associated with the different existing strategies of forcing an oceanic model, (ii) test different parameterizations of the CFB, and (iii) propose the best strategy to account for CFB in forced oceanic simulation. We show that scatterometer wind or stress are not suitable to properly represent the CFB in forced oceanic simulation. We furthermore demonstrate that a parameterization of CFB based on a wind-predicted coupling coefficient between the surface current and the stress allows us to reproduce the main characteristics of a coupled simulation. Such a parameterization can be used with any forcing set, including future coupled reanalyses, assuming that the associated oceanic surface currents are known. A further assessment of the thermal feedback of the surface wind in response to oceanic surface temperature gradients shows a weak forcing effect on oceanic currents.

Key Points:
- The Current FeedBack to the Atmosphere (CFB) can be parameterized in a forced oceanic model
- A parameterization of the CFB based on a predicted coupling coefficient is the best parameterization
- Scatterometers are not suitable to correctly represent the CFB in a forced oceanic model (unless coherent surface currents are known)

Supporting Information:
- Supporting Information S1

Correspondence to:
L. Renault,
lionel.renault@ird.fr

Citation:
Renault, L., Masson, S., Arsouze, T., Madec, G., & McWilliams, J. C. (2020). Recipes for how to force oceanic model dynamics. *Journal of Advances in Modeling Earth Systems*, *12*, e2019MS001715. https://doi.org/10.1029/2019MS001715

Received 11 APR 2019
Accepted 25 NOV 2019
Accepted article online 2 DEC 2019

1. Introduction

Resolving mesoscale eddies in oceanic models is required to quantitatively reproduce key features of the ocean circulation such as the Western Boundary Currents (Chassignet & Marshall, 2013; McWilliams, 2008), the Southern Ocean overturning (e.g., Downes et al., 2018; Hallberg & Gnanadesikan, 2006), and the total heat transport and biogeochemical variability (Colas et al., 2012; Dong et al., 2014; Gruber et al., 2011; McGillicuddy et al., 2007; Renault, Deutsch, McWilliams, et al., 2016). Meanwhile, satellite sensors such as scatterometers (e.g., QuikSCAT) have been used to better understand mesoscale air-sea interactions and to demonstrate their global ubiquity and effects on 10-m wind and surface stress (Chelton et al., 2001, 2004, 2007; Chelton & Xie, 2010; Cornillon & Park, 2001; Desbiolles et al., 2017; Gaube et al., 2015; Kelly et al., 2001; Renault, McWilliams, & Masson, 2017; O'Neill et al., 2010, 2012). They also motivated model developments and numerical studies that aim to understand the air-sea interaction effects in both the atmosphere and the ocean (Desbiolles et al., 2016; Hogg et al., 2009; Minobe et al., 2008; Oerder et al., 2016, 2018; Renault, Molemaker, McWilliams, et al., 2016; Renault, Molemaker, Gula, et al., 2016; Seo et al., 2016, 2019; Seo, 2017). So far, at the oceanic mesoscale, the scientific community has been focused on two types of air-sea interaction related to the momentum coupling: the Thermal Feedback (TFB) and the Current Feedback (CFB) to the atmosphere.

The mesoscale TFB generates wind and surface stress magnitude, divergence, and curl anomalies (Chelton et al., 2004, 2007; O'Neill et al., 2010, 2012) in response to Sea Surface Temperature (SST) gradients. Small et al. (2008) provides a review of the different processes involved. The mesoscale TFB-induced stress curl anomalies induce Ekman pumping that can have an influence on eddy propagation but not on eddy magnitude (Seo et al., 2016; Seo, 2017). Also, Ma et al. (2016) suggest that the mesoscale TFB, by causing wind velocity and turbulent heat flux anomalies, could regulate the Western Boundary Currents; however, in that study, a large spatial filter (with a spatial cutoff of more than 1000 km) is used.

CFB is another aspect of the interaction between atmosphere and ocean (Bye, 1985; Dewar & Flierl, 1987; Duhaut & Straub, 2006; Renault, Molemaker, McWilliams, et al., 2016; Rooth & Xie, 1992). In the past,

under the assumption that the oceanic current is much weaker than the wind, and maybe also because the simulated mesoscale activity was too low in low-resolution oceanic models, the CFB has been generally ignored, although forerunner studies showed that it could effect both the mesoscale and the large-scale circulations. The CFB has two main effects on the ocean circulation: (i) at the large scale, by reducing the surface stress, it slows down the mean oceanic circulation (Pacanowski, 1987; Luo et al., 2005; Renault, Molemaker, Gula, et al., 2016; Renault, McWilliams, & Penven, 2017) and (ii) at the mesoscale, the CFB induces Ekman pumping and a physically related transfer of energy from the ocean to the atmosphere (Gaube et al., 2015; Renault, McWilliams, & Masson, 2017; Scott & Xu, 2009; Xu & Scott, 2008). This process, sometimes called "top drag" (Dewar & Flierl, 1987) or "eddy killing" (Renault, Molemaker, McWilliams, et al., 2016), realistically prevents an excessive mesoscale activity in high-resolution numerical models by damping the mesoscale activity by ≈30% in kinetic energy (Oerder et al., 2018; Renault, Molemaker, McWilliams, et al., 2016; Renault, McWilliams, & Penven, 2017; Seo et al., 2016; Small et al., 2009). By a subsequent reduction of the inverse cascade of energy (i.e., a weakening of the eddy-mean flow interaction), the CFB also operates a strong control on the Western Boundary Currents, stabilizing the Gulf Stream and the Agulhas Current retroflection paths (Renault, Molemaker, Gula, et al., 2016; Renault, McWilliams, & Penven, 2017; Renault et al., 2019). At the mesoscale, the oceanic currents are very nearly geostrophic and mainly rotational (i.e., horizontally nondivergent), so that the mesoscale effect of CFB mainly affects the stress and wind curl but not systematically the stress and wind magnitude nor divergence (Chelton et al., 2004; O'Neill et al., 2003; Renault, Molemaker, McWilliams, et al., 2016; Renault et al., 2019). The surface stress and wind responses to the CFB can be characterized by coupling coefficients between the mesoscale current vorticity and stress curl (s_τ), and between the mesoscale current vorticity and wind curl (s_w). At first order, s_τ can be interpreted as a measure of the efficiency of the CFB. The more negative s_τ is, the more efficient the "eddy killing" is (Renault, McWilliams, & Masson, 2017) and, thus, the larger the damping of mesoscale activity.

When estimating the surface stress in a coupled model, the CFB is taken into account by using the wind relative to the oceanic current instead of the absolute wind neglecting surface motion (Renault et al., 2019). From an oceanic perspective, coupled simulations are computationally expensive because of the high computational cost of atmospheric models with respect to oceanic ones. Therefore, oceanic simulations are usually forced by an atmospheric product (derived from observations or numerical simulations). However, the recent finding on the role of the CFB in determining the ocean dynamics raises the following questions:

- What atmospheric forcing product should be used and how?
- When forcing the ocean with absolute wind, hence ignoring the CFB, to what extent do these simulations overestimate the mean currents and the mesoscale activity?
- How to accurately take into account the CFB in an uncoupled oceanic simulation? To what extent can the parameterizations proposed in (Renault, Molemaker, McWilliams, et al., 2016) and (Renault, McWilliams, & Masson, 2017) can mimic a coupled ocean-atmosphere model that includes the CFB?

This study first aims to quantify the biases made on the mean and mesoscale oceanic circulations when forcing an oceanic model with common reanalyses (e.g., CFSR; Saha et al., 2010) or scatterometer products (e.g., QuikSCAT; e.g., Bentamy et al., 2013), with either absolute or relative winds, and then it goes a step further than (Renault, Molemaker, McWilliams, et al., 2016) and (Renault, McWilliams, & Masson, 2017) by testing the validity of the proposed parameterizations of the wind and stress responses to the CFB. The main goal of this study is to assess to what extent a forced oceanic simulation can mimic the dynamics of a coupled simulation that includes the CFB. Quasi-global ocean-atmosphere coupled simulations (Samson et al., 2017; (Renault, Masson, et al., 2019) are first used to mimic the atmospheric forcing from scatterometers and reanalyses by generating synthetic atmospheric forcing. An additional set of uncoupled oceanic simulations is then made forced by this synthetic forcing (Section 2) using or not the parameterizations proposed by (Renault, Molemaker, McWilliams, et al., 2016) and (Renault, McWilliams, & Masson, 2017).

The following four primary diagnostics are used (Section 2):

- magnitude of the vertically integrated current;
- coupling coefficient between surface current vorticity and surface stress curl (s_τ);
- eddy wind-work sink of energy induced by the CFB ($F_e K_e$);
- mesoscale activity (Eddy Kinetic Energy, EKE).

Note that the mesoscale TFB is only briefly assessed in Section 5 and it does not appear to have a significant impact on these diagnostics.

The models and methodology are described in Section 2, and the coupled and forced simulations are presented in Section 3. Section 4 illustrates how reanalyses and scatterometer products represent the surface stress and wind responses to CFB. In Section 5, coupled simulations are analyzed to show the sensitivity of the primary diagnostic quantities with respect to the mesoscale CFB and TFB. Sections 6 and 7 assess the behavior of oceanic simulations forced by a wind or stress derived from a reanalysis and a scatterometer, respectively. In Section 8, different parameterizations of the CFB are tested. Finally, Section 9 discusses how to best force an oceanic model within a framework of future atmospheric reanalysis, that is, by using a synthetic reanalysis that takes into account the CFB. The results are discussed and summarized in Section 10.

2. Model and Methods

2.1. Coupled Ocean-Atmosphere Model

The numerical models and configurations are the same as the ones employed in Samson et al. (2017) and (Renault, Masson, et al., 2019). The following model descriptions are derived from these studies with minor modifications. The oceanic simulations were performed with the Nucleus for European Modelling of the Ocean (NEMO) v3.4 (Madec & NEMO-System-Team, 2015). The atmospheric component is the Weather Research and Forecasting (WRF) Version 3.3.1 (Skamarock et al., 2008). NEMO and WRF are coupled through the OASIS3-MCTV3 coupler (Craig et al., 2017).

The oceanic (atmospheric) component uses an Arakawa-C grid, based on a Mercator projection at 1/12° (1/4°) resolution. The geographical domain of this coupled model is a tropical channel extending from 45°S to 45°N, with the oceanic grid being a perfect subdivision by three of the atmospheric grid. The ocean vertical grid has 75 levels, with 25 levels above 100 m and a resolution ranging from 1 m at the surface to 200 m at the bottom. The atmospheric grid has 60 eta levels with a top of the atmosphere located at 50 hPa. The WRF default vertical resolution has been multiplied by three below 800 hPa. Thus, the first 33 levels are approximately located below 500 hPa with the first eta base level located at 10 m above the ocean.

As in Samson et al. (2017), the physical package we use in WRF is the longwave Rapid Radiative Transfer Model (RRTM; Mlawer et al. (1997), the "Goddard" Short Wave (SW) radiation scheme (Chou & Suarez, 1999), the "WSM6" microphysics scheme (Hong & Lim, 2006), the Betts-Miller-Janjic (BMJ) convection scheme (Betts & Miller 1986; Janjić, 1994), the Yonsei University (YSU) planetary boundary layer scheme (Hong et al., 2006), the unified NOAH Land Surface Model (LSM) with the surface layer scheme from MM5 (Chen & Dudhia, 2001). The planetary boundary layer scheme MYNN2.5 (Nakanishi & Niino, 2006) is also used instead of YSU in an additional specific simulation. Note that in WRF (since Version 3.3.1), the YSU scheme has been modified following Shin et al. (2012) to overcome issues related to a first eta level situated around 10-m. WRF lateral boundary conditions are prescribed from the European Centre for Medium-Range Weather Forecasts ERA-Interim 0.75° resolution reanalysis (Dee et al., 2011) at 6-hourly intervals.

The ocean physics used in NEMO corresponds to the Upstream-Biased Scheme (UBS; Shchepetkin & McWilliams, 2009) advection for the tracers and the dynamics with no explicit diffusivity and viscosity. The vertical eddy viscosity and diffusivity coefficients are computed from a TKE turbulence closure model (Blanke & Delecluse, 1993). The surface boundary condition on momentum is the surface stress, which is applied as the surface boundary condition on the momentum vertical mixing. The oceanic open boundary conditions are prescribed with an interannual global $\frac{1}{4}^\circ$ DRAKKAR simulation (Brodeau et al., 2010). In order to benefit, at a limited cost, from a fully spun-up mesoscale circulation in the initial conditions of the $\frac{1}{12}^\circ$ ocean, we first run a 5-year forced ocean simulation initialized from $\frac{1}{4}^\circ$ DRAKKAR simulations.

2.2. Forced Oceanic Model

To be able to compare the forced simulations to the coupled simulations, it is crucial to have an oceanic model configuration as close as possible to the coupled simulations configuration. Therefore, the forced ocean simulations were performed with NEMO 3.4 using the very same configuration and the exact same initial condition as the coupled simulations. All the forced simulations described hereafter differ only in the atmospheric forcing used or the way they estimate the surface stress. In order to run forced ocean simulations with characteristics as close as possible to the coupled model simulations, we had to modify the bulk formula available in NEMO 3.4. To do so, we used the AeroBulk package (Brodeau et al., 2017, now included in NEMO v4), which offers the possibility to use the bulk formula COARE v3.0 (Fairall et al., 2003), as in our

coupled simulations that use the WRF bulk formulae. We also used hourly forcing fields, which corresponds to the coupling frequency of the coupled simulations. The numerical outputs for the solutions are daily averages.

2.3. Surface Wind and Stress

In a forced oceanic model, surface wind stress is either directly prescribed or computed from wind usually taken at 10 m to be compliant with the parameters used in the bulk formulae. Two kinds of prescribed 10-m winds can be defined:

- $\boldsymbol{U_{10abs}}$: the absolute wind at 10 m,
- $\boldsymbol{U_{10rel}}$: the 10 m wind relative to the oceanic surface current: $\boldsymbol{U_{10rel}} = \boldsymbol{U_{10abs}} - \boldsymbol{U_o}$.

Usually, the atmospheric models (such as WRF) provide a 10-m wind diagnostic (U10 and V10 in WRF), which represents in fact $\boldsymbol{U_{10rel}}$ when ocean surface currents seen by the atmosphere are not set to zero (see also (Renault, Masson, et al., 2019). $\boldsymbol{U_{10abs}}$ can be simply reconstructed by adding up $\boldsymbol{U_o}$ to $\boldsymbol{U_{10rel}}$. The surface stress is computed in WRF based on $u*$, the friction velocity defined in the Monin-Obukhov similarity theory. Because the same vertical scaling, based on the Monin-Obukhov length scale, is used to compute $u*$ and (U10,V10) from the first layer model information, the surface stress can be given as a function of variables given either at 10 m or at the first level of the model. When the surface current is taken into account in WRF, the surface stress is therefore defined by the following equation:

$$\boldsymbol{\tau} = \rho_a C_D(\boldsymbol{U_{10abs}} - \boldsymbol{U_o})|\boldsymbol{U_{10abs}} - \boldsymbol{U_o}| = \rho_a C_D \boldsymbol{U_{10rel}}|\boldsymbol{U_{10rel}}|. \quad (1)$$

Note that to properly take into account the impact of the oceanic surface current in the atmosphere, we must also modify the tridiagonal matrix system solved in the vertical turbulent diffusion scheme (Lemarié, 2015; Renault, Lemarié, & Arsouze, 2019).

If the surface currents are considered as zero in WRF, the same equation applies but with $\boldsymbol{U_o} = 0$, implying $\boldsymbol{U_{10rel}} = \boldsymbol{U_{10abs}}$ and so

$$\boldsymbol{\tau} = \rho_a C_D \boldsymbol{U_{10abs}}|\boldsymbol{U_{10abs}}|. \quad (2)$$

Scatterometer winds are estimated from the pseudo-stress and are also reported as a 10-m equivalent neutral wind relative to the oceanic current, that is, a relative wind to the oceanic current that would exist if the conditions were neutrally stable (Plagge et al., 2012). The 10-m equivalent neutral wind long-term mean is very similar to the 10-m long-term mean (not shown). However, at the mesoscale, because atmospheric stratification can deviate significantly from neutral conditions, the 10-m equivalent neutral wind response to the TFB and to the CFB can be overestimated by 10% to 25% with respect to 10-m wind response (O'Neill et al., 2012; Perlin et al., 2014; Song et al., 2009). Note that an oceanic simulation forced by such a wind product is not affected by this mesoscale overestimation as the simulated eddies are not correlated with those that have been seen by the scatterometers.

2.4. Spatial Filtering

As in Seo (2017) and (Renault, Masson, et al., 2019), the mesoscale anomalies are isolated from the large-scale signal by using a spatial filter. The following filter description is derived from (Renault, Masson, et al., 2019) with minor modifications. A field ϕ is smoothed using a Gaussian spatial filter with a standard deviation σ of 4 (12) grid points at 1/4° (1/12°). Gaussian weights of points located at a distance larger than 3σ are considered zero. The Gaussian filter is thus applied on a $(6\sigma + 1) \times (6\sigma + 1)$ window, which makes 25×25 points at 1/4°, or 73×73 points at 1/12°, and corresponds to 670 km (475 km) at the equator (45°N) because of the Mercator projection (grid size scales with the cosin of the latitude). One of the properties of the Gaussian filter is that its Fourier transform, and so its spatial frequency response is also a Gaussian function. This allows an analytical definition of the cutoff wave number for a given reduction of the filter response. For example, the power spectrum of the filtered signal will be half of the original signal (−3 dB) at the wave number of about 1/600 km^{-1} at the equator and 1/420 km^{-1} at 45°N. It will be divided by 10 (−10 dB) at the wave number of about 1/330 km^{-1} at the equator and 1/280 km^{-1} at 45°N. Land points are treated as missing data, and the weights of windows including land points are renormalized over the remaining oceanic points. Mesoscale anomalies of a field ϕ are then defined as $\phi' = \phi - [\phi]$, with $[\phi]$ the smoothed field. This filter is applied on one coupled simulation (see Section 3) and to the coupling coefficients described hereafter (see Section 2.6).

2.5. Mean Oceanic Circulation

The CFB causes a slowdown of the mean oceanic circulation. To characterize this effect in our simulations, the magnitude of the vertically integrated current (m^2/s) is estimated as

$$V_{5y} = \sqrt{\overline{\int_H^\eta u dz}^2 + \overline{\int_H^\eta v dz}^2}, \tag{3}$$

where the mean $\bar{\cdot}$ is defined with respect to long-term temporal averaging (5 years of simulations), u and v are the zonal and meridional currents at each depth, and H the bottom of the ocean. V_{5y} is the barotropic transport that flows through a section of 1 m long that is perpendicular in any point to the barotropic flow. To assess the temporal evolution of the mean circulation, the magnitude of the vertically integrated current (m^2/s) is also estimated using a 3-month running window:

$$V_{3m} = \sqrt{\left\langle \int_H^\eta u dz \right\rangle^2 + \left\langle \int_H^\eta v dz \right\rangle^2}, \tag{4}$$

where the mean $< \cdot >$ is defined with respect to the 3-month running window. Note that the estimation of the magnitude of the vertically integrated current is nonlinear. As a result, a long-term temporal average of V_{3m} is systematically stronger than V_{5y}.

2.6. CFB Coupling Coefficients

As in (Renault, McWilliams, & Masson, 2017) and (Renault, Masson, et al., 2019), the coupling coefficient between mesoscale current vorticity and surface stress curl s_τ is defined as the slope of the robust regression (Maronna et al., 2006) between surface stress curl and oceanic current vorticity. Following (Maronna et al., 2006), our M-estimation is based on a biweight function. s_τ is evaluated at each grid point. In order to isolate the stress response due to the mesoscale oceanic surface current, the fields are first temporally averaged using a 29-day running mean to suppress the weather-related variability (Chelton et al., 2007), and the large-scale signal is removed using a high-pass Gaussian spatial filter (as in, e.g., Seo, 2017; see filter description in Section 2d). Note that a, for example, 15-day running mean does not efficiently suppress the weather-related variability. (Renault, Masson, et al., 2019) demonstrate s_τ properly isolates the stress response to the CFB from the TFB. The coupling coefficient s_w is estimated as s_τ but using U_{10abs} instead of the surface stress.

2.7. Sink of Oceanic Energy by the Mesoscale CFB

The CFB induces transfers of energy from the mesoscale oceanic currents to the atmosphere. These sinks of oceanic energy are crucial to represent in a oceanic model as they partly control the oceanic mesoscale activity. Temporal filters are commonly used to estimate the eddy work. However, they do not allow proper isolation of the sinks of energy induced by the CFB, because the characteristic lifetime of ocean eddies (usually >90-day) does not allow to filter out wind stress with large spatial scales. In this study, in order to isolate these sinks of energy, we define the mesoscale (eddy) wind work F_eK_e [$m^3\ s^{-3}$] using a spatial filter:

$$F_eK_e = \frac{1}{\rho_0}\left(\overline{\tau'_x\, U'_o} + \overline{\tau'_y\, V'_o}\right), \tag{5}$$

where the mean $\overline{\cdot}$ is defined with respect to long-term averaging (5 years of simulations) and $'$ is defined as the signal anomalies as estimated using the spatial filter described in Section 2d. Note that this spatial-filter-based definition differs from the usual Reynolds decomposition. For instance, cross-terms do not completely vanish (but remain very weak; see the supporting information). However, it allows better isolation of the oceanic mesoscale signal from large-scale currents that can have a duration of, for example, less than 1 month (e.g., wind-driven current). Nevertheless, similar results can be found using a temporal filter and by estimating difference between a simulation with CFB and a simulation without CFB (Jullien et al., 2020).

2.8. Eddy Kinetic Energy

The Eddy Kinetic Energy (EKE, [m^2/s]) represents the intensity of the mesoscale activity. In this study, it is computed from the geostrophic currents anomalies estimated using the filter described above.

$$EKE = \overline{\frac{1}{2}\sqrt{U_o'^2 + V_o'^2}}. \quad (6)$$

Again, this spatial-filter-based definition of EKE differs from the usual Reynolds decomposition, and cross-terms such as $\bar{U}'$ do not vanish over standing eddies.

3. Coupled and Forced Simulations

We define the following naming convention to identify the different coupled and forced simulations performed:

- The first capital letter defines the type of atmospheric forcing used: *C* is a coupled simulation; *R* stands for Reanalysis (as mimicked by a coupled simulation), that is, atmospheric data derived from a coupled simulation; and *Sc* stands for Scatterometer (as mimicked by a coupled simulation).
- The first subscript word indicates whether the coupled model data used for forcing takes into account or not the CFB (i.e., *CFB* or *NOCFB*).

The following is the case of forced simulations only:

- The second capital letter indicates if the surface stress used to force the the ocean model dynamics is directly prescribed (*S*) or computed in the ocean model bulk formulae from a prescribed wind speed (*W*).
- In simulations using bulk formulae to compute the wind stress, the following lowerscript, *REL* or *ABS*, indicates whether we use a wind relative to currents of the forced ocean simulation or not.

Finally, when relevant, a third capital letter *P* indicates that a parameterization for the wind response is used in forced simulations, followed by the name of the parameterization in subscript (see Section 3.4 for more details).

3.1. Coupled Simulations

As described in Table 1, two reference 5-year coupled simulations are performed over the 1989–1993 period, only differing by their degree of coupling:

- In C_{CFB}, WRF gives NEMO hourly averages of freshwater, heat, and momentum fluxes, whereas the oceanic model sends back to WRF the hourly averaged Sea Surface Temperature (SST) and surface currents. The surface stress is estimated using the wind relative to the oceanic current $\boldsymbol{U}_{10rel}$.
- In C_{NOCFB}, the oceanic model sends back to WRF only the SST. WRF sees zero surface current and the surface stress is a function of $\boldsymbol{U}_{10abs}$.

Another simulation has been carried out to briefly assess the mesoscale TFB impact on the mean and mesoscale oceanic circulations:

- In C_{CFB_SMTH}, the setup is the same than for C_{CFB} except that the SST sent to WRF is spatially filtered (see description of the filter in Section 2) in order to smooth out the thermal mesoscale structures. C_{CFB_SMTH} thus contains the CFB and the large-scale TFB (as in, e.g., Seo, 2017). This simulation is used to briefly assess the mesoscale TFB impact on the mean and mesoscale oceanic circulations.

Additional coupled simulations have been carried out to assess the sensitivity of the results to the physics taken into account in the model and to the internal variability of the oceanic model (see the supporting information):

- The simulation C_{CFB_MYNN} is the same than C_{CFB} except that the MYNN2.5 (Nakanishi & Niino, 2006) Planetary Boundary Layer scheme is used instead of YSU in the atmospheric model. It allows an assessment of the sensitivity of the results to the Planetary Boundary Layer used in the atmospheric model in Supplemental Information.
- Two more coupled simulations identical to C_{CFB} have been run on different machines and using different compiler options of optimization (C_{CFB2}, C_{CFB3}). This adds very small perturbations all along the simulation run. This set of three identical coupled simulations defines a small ensemble that is used to provide an estimate of the robustness of the results and of the role of the internal variability in the models (see also Figures S2 and S3). Note that because of the small number of experiments, the internal variability may be underestimated.

Table 1
Main Experiments

Forcing product	Way to force	Use of parameterization for wind response	Type of parameterization	Stress formulae	Name of the simulation
Coupled (C)	CFB	NO		$\boldsymbol{\tau} = \rho_a C_D \boldsymbol{U_{10rel}} \lvert \boldsymbol{U_{10rel}} \rvert$	C_{CFB}
	NOCFB	NO		$\boldsymbol{\tau} = \rho_a C_D \boldsymbol{U_{10abs}} \lvert \boldsymbol{U_{10abs}} \rvert$	C_{NOCFB}
	CFB (smoothed SST)	NO		$\boldsymbol{\tau} = \rho_a C_D \boldsymbol{U_{10rel}} \lvert \boldsymbol{U_{10rel}} \rvert$	C_{CFB_SMTH}
Reanalysis-like produced without CFB (R_{NOCFB}), $\boldsymbol{U_{10abs}}$ or $\boldsymbol{\tau_{pNOCFB}}$	Stress	NO		$\boldsymbol{\tau} = \boldsymbol{\tau_{pNOCFB}}$	$R_{NOCFB}S$
	ABS (Wind)	NO		$\boldsymbol{\tau} = \rho_a C_D \boldsymbol{U_{10abs}} \lvert \boldsymbol{U_{10abs}} \rvert$	$R_{NOCFB}W_{ABS}$
	REL (Wind)	NO		$\boldsymbol{\tau} = \rho_a C_D (\boldsymbol{U_{10abs}} - \boldsymbol{U_o}) \lvert \boldsymbol{U_{10abs}} - \boldsymbol{U_o} \rvert$	$R_{NOCFB}W_{REL}$
	s_w	Prescribed - Constant	$\boldsymbol{\tau} = \rho_a C_D (\boldsymbol{U_{10abs}} - (1-s_w)\boldsymbol{U_o}) \lvert \boldsymbol{U_{10abs}} - (1-s_w)\boldsymbol{U_o} \rvert$	$R_{NOCFB}W_{REL}Ps_wC$
		Prescribed. - Monthly maps	$\boldsymbol{\tau} = \rho_a C_D (\boldsymbol{U_{10abs}} - (1-s_w)\boldsymbol{U_o}) \lvert \boldsymbol{U_{10abs}} - (1-s_w)\boldsymbol{U_o} \rvert$	$R_{NOCFB}W_{REL}Ps_wM$
	Stress	s_τ	Prescribed - monthly maps	$\boldsymbol{\tau} = \boldsymbol{\tau_{pNOCFB}} + s_\tau \boldsymbol{U_o}$	$R_{NOCFB}SPs_\tau M$
			Predicted	$\boldsymbol{\tau} = \boldsymbol{\tau_{pNOCFB}} + s_\tau \boldsymbol{U_o}$	$R_{NOCFB}SPs_\tau P$
Reanalysis-like produced with CFB (R_{CFB}), $\boldsymbol{U_{10abs}}$ or $\boldsymbol{\tau_{pCFB}}$	ABS (Wind)	NO		$\boldsymbol{\tau} = \rho_a C_D \boldsymbol{U_{10abs}} \lvert \boldsymbol{U_{10abs}} \rvert$	$R_{CFB}W_{ABS}$
	Stress	s_τ	Predicted	$\boldsymbol{\tau} = \boldsymbol{\tau_{pCFB}} + s_\tau (\boldsymbol{U_o} - \boldsymbol{U_{orea}})$	$R_{CFB}SPs_\tau P$
	REL (Wind)	NO		$\boldsymbol{\tau} = \rho_a C_D (\boldsymbol{U_{10abs}} - \boldsymbol{U_o}) \lvert \boldsymbol{U_{10abs}} - \boldsymbol{U_o} \rvert$	$R_{CFB}W_{REL}$
Scatterometer -like (Sc) from C_{CFB}, $\boldsymbol{U_{10rel}}$ or $\boldsymbol{\tau_{pCFB}}$	Stress	NO		$\boldsymbol{\tau} = \boldsymbol{\tau_{pCFB}}$	$Sc_{CFB}S$
	ABS (Wind)	NO		$\boldsymbol{\tau} = \rho_a C_D \boldsymbol{U_{10rel}} \lvert \boldsymbol{U_{10rel}} \rvert$	$Sc_{CFB}W_{ABS}$
	REL (Wind)	NO		$\boldsymbol{\tau} = \rho_a C_D (\boldsymbol{U_{10rel}} - \boldsymbol{U_o}) \lvert \boldsymbol{U_{10rel}} - \boldsymbol{U_o} \rvert$	$Sc_{CFB}W_{REL}$

Note. All the experiments consider the large-scale thermal feedback.

3.2. Mimicking Atmospheric Reanalysis

To mimic the different ways of forcing an oceanic model with a reanalysis, five forced oceanic simulations are carried out (see also Table 1):

- $R_{NOCFB}S$: The model is forced by a surface stress τ_{pNOCFB} that is directly provided by C_{NOCFB}, that is, a simulation that did not feel the CFB. The surface stress used in this simulation mimics that from a reanalysis such as CFSR or ERA-Interim.
- $R_{NOCFB}W_{ABS}$: The model is forced by $\boldsymbol{U_{10abs}}$ derived from C_{NOCFB}, mimicking $\boldsymbol{U_{10abs}}$ from a reanalysis such as CFSR or ERA-Interim. The stress is estimated in the NEMO bulk formulae without taking into account the surface currents of the forced simulation (W_{ABS}).
- $R_{CFB}W_{ABS}$: The model is forced by $\boldsymbol{U_{10abs}}$ derived from C_{CFB}, that is, a simulation that felt the CFB. $\boldsymbol{U_{10abs}}$ mimics the wind that could be provided by future reanalysis (that would take into account the CFB) or by a regional atmospheric simulation that takes into account the CFB. The surface currents of the forced simulation are not taken into account when estimating the stress in the NEMO bulk formulae (W_{ABS}).
- $R_{NOCFB}W_{REL}$: Same as $R_{NOCFB}W_{ABS}$, the stress is estimated using $\boldsymbol{U_{10abs}}$ from C_{NOCFB}, but relative to the surface currents simulated by the oceanic forced simulation.
- $R_{CFB}W_{REL}$: Same as $R_{CFB}W_{ABS}$, the stress is estimated using $\boldsymbol{U_{10abs}}$ from C_{CFB}, but relative to the surface currents simulated by the oceanic forced simulation.

An additional simulation forced by the stress from a reanalysis that felt the CFB could be done, but it would correspond to the $Sc_{CFB}S$ simulation described hereafter. Note that all the forced oceanic simulations using NEMO bulk formulae and presented in this subsection use $\boldsymbol{U_{10abs}}$.

3.3. Mimicking Scatterometer Winds

We saw in Section 2.3 that scatterometer winds can lead to two different errors: an overestimation of the coupling coefficient between mesoscale surface current vorticity and wind curl and a slightly larger long-term averaged wind. However, when forcing an oceanic model with scatterometer wind (and without data assimilation), because the simulated eddies are not correlated with those that have been seen by the scatterometers, the main source of error therefore lies in the fact that the long-term mean of equivalent neutral scatterometer wind is relative to the oceanic motions. In the following experiments, for simplicity and to limit the number of close experiments, $\boldsymbol{U_{10rel}}$ is used instead of the equivalent neutral wind relative to the oceanic current. The use of the equivalent neutral wind relative to the oceanic motions would lead to similar results.

To mimic the different way of forcing an oceanic model with a scatterometer product, three more simulations are carried out (see also Table 1):

- $Sc_{CFB}S$: The model is forced by a surface stress τ_{pCFB} that is directly provided by C_{CFB}, that is, a simulation that felt the CFB. The forcing mimics scatterometer surface stress.
- $Sc_{CFB}W_{ABS}$: The model is forced by an $\boldsymbol{U_{10rel}}$ wind derived from C_{CFB}, mimicking scatterometer wind. This wind is relative to the oceanic current simulated by the C_{CFB}. The surface currents of the forced simulation are not taken into account when computing the wind stress from $\boldsymbol{U_{10rel}}$ in NEMO bulk formulae (W_{ABS}).
- $Sc_{CFB}W_{REL}$: Same as $Sc_{CFB}W_{ABS}$ but the surface currents of the forced simulation are taken into account when computing the wind stress from $\boldsymbol{U_{10rel}}$ in NEMO bulk formulae (W_{REL}).

Note that although atmospheric products that incorporate scatterometer winds such as CFSR or JRA55-do (Tsujino et al., 2018) should act in a similar way as QuikSCAT, they do not strongly resemble scatterometer data, for example, at ocean fronts, suggesting that the assimilation does not strongly constrain the near-surface JRA55-do (Abel, 2018).

3.4. Parameterizing CFB in a Forced Oceanic Model

(Renault, Molemaker, McWilliams, et al., 2016) and (Renault, McWilliams, & Masson, 2017) have identified relationships linking the wind and stress response to the oceanic surface currents. To mimic the CFB in a forced oceanic model, they suggest a wind-correction approach or a stress-correction approach. We propose now to test the different approaches in ad hoc parameterizations using atmospheric wind derived from the coupled simulations.

3.4.1. The Wind-Correction Approach

(Renault, Molemaker, McWilliams, et al., 2016) suggest a simple parameterization based on the current-wind coupling coefficient s_w (see Section 2.6) estimated from a coupled simulation (C_{CFB}). s_w corresponds to the linear wind response to a given current:

$$\boldsymbol{U'_a} = s_w \boldsymbol{U_o}, \tag{7}$$

where $\boldsymbol{U_o}$ is the surface current and $\boldsymbol{Ua'}$ is the wind response to $\boldsymbol{U_o}$. If the wind cannot see the surface current, then $s_w = 0$ (no wind response to the current). If $s_w = 1$, in a forced ocean model, this would be an ideal case, in which there is no loss of energy; that is, the current generates a wind response with a magnitude equal to the current magnitude. When forcing an oceanic model with a product that did not account for CFB, the surface stress should be computed with a wind relative to the current corrected by s_w: $\boldsymbol{U_{10abs}} - (1 - s_w)\boldsymbol{U_o}$, which is then used to obtain $\boldsymbol{\tau}$ in the bulk formula (1). Two forced simulations are carried out using this parameterization. The first letter of the simulation name stands for parameterization; the second letter indicates the kind of parameterization used:

- $R_{NOCFB}W_{REL}Ps_wC$: a simulation with a constant $s_w = 0.3$, which corresponds to the global mean value of s_w as estimated from C_{CFB}. $\boldsymbol{U_{10abs}}$ is derived from C_{NOCFB}.
- $R_{NOCFB}W_{REL}Ps_wM$: a simulation that takes into account monthly and spatial variations of s_w. In this simulation, the monthly maps of s_w, estimated from C_{CFB}, are provided to the oceanic simulation. $\boldsymbol{U_{10abs}}$ is derived from C_{NOCFB}.

3.4.2. The Stress-Correction Approach

Alternatively, (Renault, McWilliams, & Masson, 2017) proposed another simple parameterization based on the current-stress coupling coefficient s_τ (see Section 2.6), in a forced oceanic model:

$$\boldsymbol{\tau} = \boldsymbol{\tau_0} + \boldsymbol{\tau'}, \tag{8}$$

where $\boldsymbol{\tau}$ is the surface stress that includes the CFB effect, $\boldsymbol{\tau_0}$ is the surface stress that does not include the CFB effect (it can be prescribed or estimated within a bulk formulae), and $\boldsymbol{\tau'}$ is the stress response to $\boldsymbol{U_o}$:

$$\boldsymbol{\tau'} = s_\tau \boldsymbol{U_o}. \tag{9}$$

s_τ can be estimated from a coupled simulation (here C_{CFB}) or, as demonstrated by (Renault, McWilliams, & Masson, 2017), can be predicted using the magnitude of the wind:

$$s_\tau = \alpha |U_{10abs}| + \beta, \tag{10}$$

with $\alpha = -2.9 \times 10^{-3}$ N s^2/m^4, and $\beta = 0.008$ N s/m^3. α and β are derived from the linear regression between $|\boldsymbol{U_{10abs}}|$ and s_τ and have uncertainties in the range of 20% (see the supporting information). Additionally, for weak wind (i.e., <3 m/s), the regression is not valid anymore and s_τ is taken as a constant of -0.0007 N s/m^3 that corresponds to its value at 3 m/s. Note that (10) can also be estimated from the observations; however, such an estimation suffers from large uncertainties (Renault, McWilliams, & Masson, 2017) because it is based on two different products (AVISO, Ducet et al., 2000, and QuikSCAT, Bentamy et al., 2013), which do not have the same effective spatial resolution. This parameterization (10) represents more physics than using (9) with a time-invariant or climatological s_τ as it allows us to represent the spatial and temporal variations of s_τ and, contrarily to s_w, does not suffer the quadratic errors induced by the bulk formula. It is also very flexible as it can be used on top of a prescribed wind stress τ_p or a stress estimated from the absolute wind in a bulk formula. For the main simulations that use a parameterization based on s_τ, the atmospheric stress used to force the model is derived from the C_{NOCFB} simulation, that is, an atmospheric simulation that did not previously feel the CFB. Based on s_τ parameterization, two simulations are carried out (see also Table 1). Again, the first letter of the simulation name stands for parameterization; the second letter indicates the kind of parameterization used:

- $R_{NOCFB}SPs_\tau M$: A simulation that is forced by a surface stress τ_{pNOCFB} and that considers monthly and spatial variations of s_τ derived from C_{CFB}.
- $R_{NOCFB}SPs_\tau P$: A simulation that is forced by a surface stress τ_{pNOCFB} and estimates s_τ using $|\boldsymbol{U_{10abs}}|$ (10).

Note that estimating the stress in the ocean model using $\boldsymbol{U_{10abs}}$ instead of a prescribed surface stress would lead to similar results. As detailed in Section 9, a final forced experiment $R_{CFB}SPs_\tau P$ has been carried out using the parameterization (10) but with an atmospheric stress forcing τ_{pCFB} as derived from C_{CFB}. This experiment mimics a reanalysis that felt the CFB (*e.g.,* Coupled-ECMWF reanalyses CERA-SAT and CERA-20C).

4. Representation of the Surface Stress and Wind Curl in Reanalyses and Scatterometer Products

Scatterometers are fundamentally stress-measuring instruments. They have been extensively used to characterize the air-sea interactions (Chelton et al., 2007; O'Neill et al., 2012; Renault, Masson, et al., 2019) and also to force oceanic models by using their derived wind or stress. Surface stress derived from scatterometer such as QuikSCAT incorporates all the ocean-atmosphere interactions, including the CFB effect on the stress (Chelton et al., 2004; Cornillon & Park, 2001; Kelly et al., 2001; Renault, McWilliams, & Masson, 2017; Renault, Masson, et al., 2019). As illustrated in Figure 1a and previously shown by Chelton et al. (2001), the surface currents have a significant imprint on the surface stress curl around the Gulf Stream path where a negative current vorticity causes a positive stress curl anomaly. As a result, on the western side of the Gulf Stream, the mean surface stress curl is negative, whereas it is positive on the other side. The wind response to the CFB should have the opposite sign than the stress response (Renault, Molemaker, McWilliams, et al., 2016). However, consistent with (Renault, Masson, et al., 2019) and as illustrated in Figure 1b, because scatterometer winds are $\boldsymbol{U_{10rel}}$, its response to the CFB has the wrong sign, misdiagnosing an increase of the wind over the Gulf Stream instead of a decrease.

Global reanalyses such as CFSR (Saha et al., 2010) or ERA Interim (Dee et al., 2011); or a simulation such as C_{NOCFB}) are commonly used to force an oceanic model. CFSR couples ocean model SST to the atmosphere, but not ocean currents, whereas ERA Interim is atmosphere only with prescribed SST. Although both reanalyses assimilate data, they do not represent the current imprint on the surface stress nor wind (Belmonte Rivas & Stoffelen, 2019). This is illustrated in Figures 1c and 1d: over the Gulf Stream, because

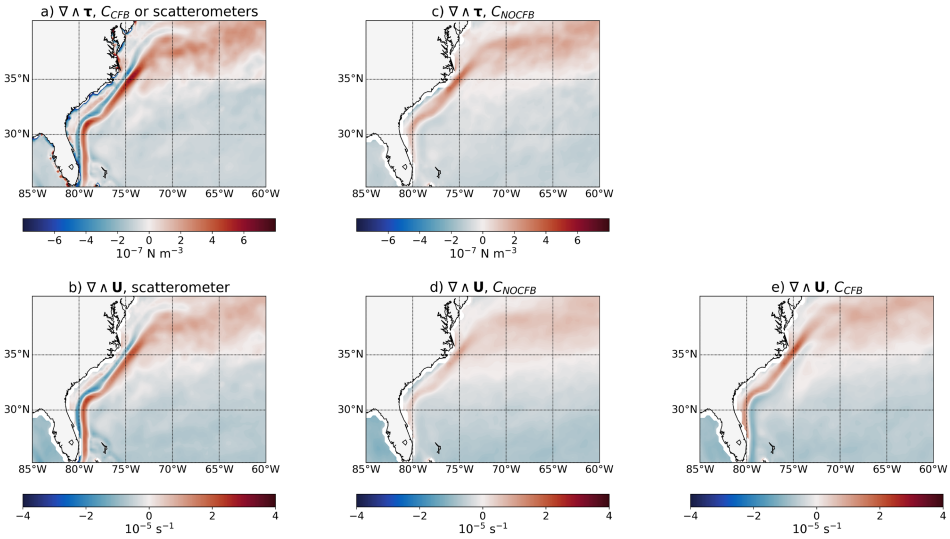

Figure 1. Long-term mean of surface stress and 10-m wind curl over the Gulf Stream region. (a) Mean surface stress curl as estimated from C_{CFB} and given to the experiments $Sc_{CFB}S$ and $R_{CFB}SPS_{\tau}P$. This is similar to the stress curl monitored by scatterometer (*i.e.,* relative wind). (b) Mean 10-m wind curl as estimated from C_{CFB} mimicking scatterometer and given to the experiments $Sc_{CFB}W_{ABS}$ and $Sc_{CFB}W_{REL}$. (c) Mean surface stress curl as estimated from C_{NOCFB} (similar to classic reanalyses products and given to the reanalysis-like simulations). (d) Similar to (c) but for the mean 10-m wind curl. (e) Similar to (d) but as estimated from C_{CFB}.

of the lack of CFB, these kind of reanalysis do not represent the imprint of the currents on the wind nor on the stress (but do represent the TFB effect). Some global coupled models (or simulations such as C_{CFB} and recent reanalysis such as CERA-SAT or CERA-20C) take into account the CFB. In such simulations, both surface stress and wind are more realistic as they are marked by the presence of the surface currents: consistent with scatterometer stress, the surface stress curl is marked by dipole of negative and positive stress curl (Figure 1a). The same behavior can be observed to a lesser extent in wind curl (with opposite signs) with more of a positive sign (Figure 1e) than a negative sign. Similar results can be found at the mesoscale over, for example, an eddy or a filament.

5. Reference Coupled Simulation C_{CFB}

5.1. CFB Effect at the Large Scale

V_{5y} from C_{CFB} is represented in Figure 2a. The main ocean circulation features are seen in C_{CFB} as, for example, the equatorial currents, the mean gyres, and the Western Boundary Currents. As revealed by the regression between V_{5y} from C_{NOCFB} and C_{CFB} (Table 2), although C_{CFB} and C_{NOCFB} simulations have a very similar mean circulation pattern, C_{NOCFB} tends to slightly overestimate its strength (see Figure 2b). This is confirmed by Figure 2b that shows the box plots of V_{5y} as estimated from the coupled simulations. Consistently, from C_{NOCFB} to C_{CFB}, the V_{5y} distribution is shifted down because the CFB reduces the mean surface stress and slows down the mean currents (Luo et al., 2005; Pacanowski, 1987). As a result, the mean and median V_{5y} are both overestimated in C_{NOCFB} by ≈ 8% with respect to C_{CFB} (see also Table 3), which is larger than the internal variability (less than 2.5%, estimated from simulations C_{CFB}, C_{CFB2}, C_{CFB3}) Figure 3a represents the monthly evolution of V_{3m}. Starting from the same initial state, it confirms that the CFB, by reducing the surface stress, induces a slow down of the mean circulation. C_{CFB} and C_{NOCFB} differ after only a couple of months and the difference between V_{3m} from C_{CFB}, and C_{NOCFB} is relatively stable after ≈10 months: V_{3m} in C_{NOCFB} is ≈11% larger than C_{CFB}.

5.2. CFB Effect at the Mesoscale

The spatial distribution of the long-term average s_{τ} from C_{CFB} is illustrated in Figure 4a. Figure 5a depicts the box plots of s_{τ} from C_{CFB}, and C_{NOCFB}. (Renault, Masson, et al., 2019) provide a full assessment of s_{τ} as simulated by C_{CFB}. s_{τ} shows temporal and spatial variability, which is driven by the 10-m wind: The larger the wind, the more negative the s_{τ} (Renault, McWilliams, & Masson, 2017). The larger values of s_{τ} are therefore mainly situated in the high-latitude regions. On a long-term average, in C_{CFB}, it varies from approximately

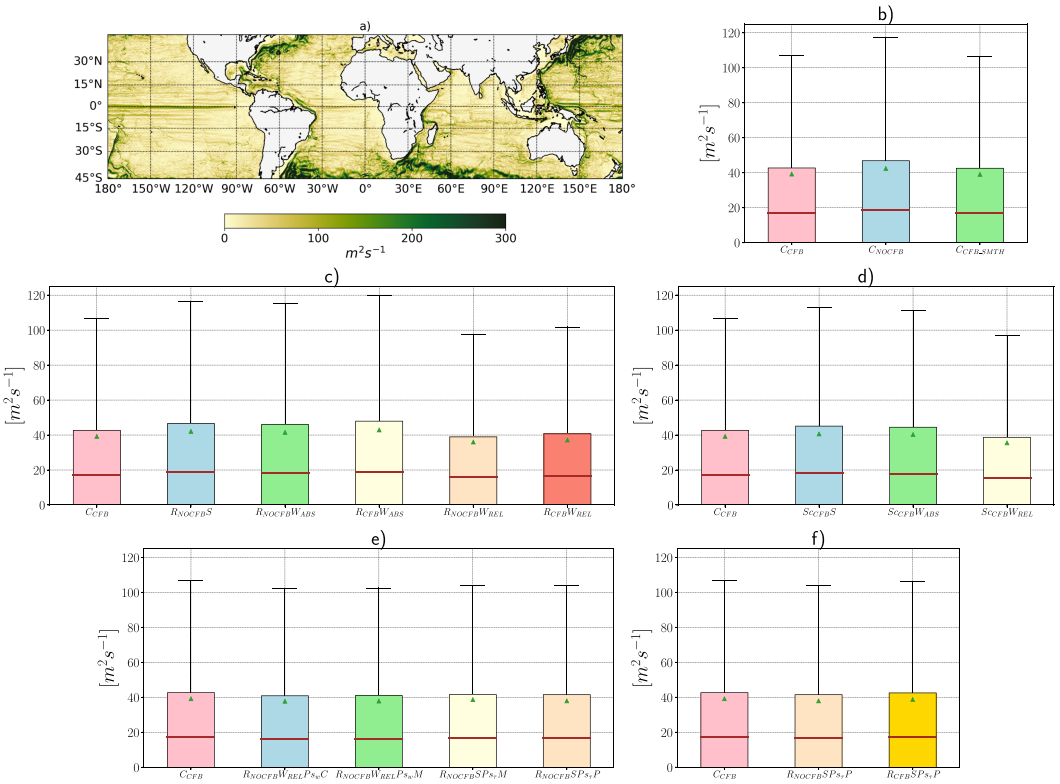

Figure 2. (a) V_{5y} [m^2 s^{-1}](Section 2) in C_{CFB}. Box plots of the spatial variability of V_{5y} from (b) coupled simulations, (c) reanalysis-like simulations, (d) scatterometer-like simulations, (e) parameterized simulations, and (f) the parameterized simulations $R_{NOCFB}SPs_\tau P$ and $R_{CFB}SPs_\tau P$. The box plot of V_{5y} estimated from C_{CFB} is shown in all the box plots for clarity. The line that divides the box into two parts represents the median of the data, whereas the green dot represents its mean. The length of the box shows the upper and lower quartiles. The extreme lines represent the 95^{th} percentiles of the distributions. The 5^{th} percentiles have values so close to 0 (due to large areas very close to zero) that they are located on the x axis and are therefore not visible. Statistical significance of the medians and means shown in the box plots have been tested with a bootstrap method. For all the box plots depicted here and in the following figures, the 95 medians are indistinguishable from the symbol used.

-0.03 to approximately 0 N s/m^3. Consistent with the literature, in C_{NOCFB}, that is, a simulation that ignores the CFB, $s_\tau \approx 0$.

Figure 6a depicts the spatial distribution of F_eK_e as estimated from C_{CFB}, and Figure 7a represents the box plots of F_eK_e as simulated by C_{CFB} and C_{NOCFB}. In agreement with, for example, Xu and Scott (2008) and (Renault, McWilliams, & Masson, 2017), in C_{CFB} F_eK_e is negative almost everywhere, expressing the large-scale sinks of energy induced by the CFB. In a coupled simulation that neglects the CFB, even if the TFB is taken into account (i.e., C_{NOCFB}), $F_eK_e \approx 0$. In C_{CFB} F_eK_e has a global mean and a median of -3.9×10^{-7} m^3/s^3 and -1.3×10^{-7} m^3/s^3 (Table 3). The largest sinks of energy are confined to the 5^{th} percentile of the distribution (Figure 7a and Table 4). They reveal locations that are characterized by an intense mesoscale activity and a notably negative s_τ and actually roughly represent the Western Boundary Currents and the Agulhas Return Current. Over these regions F_eK_e has a mean and a median of -37.7×10^{-7}m^3/s^3 and 26.8 $\times 10^{-7}$m^3/s^3, respectively.

The spatial distribution of the EKE from C_{CFB} is illustrated in Figure 8a; it shows a general agreement with the literature. Figure 9a shows the box plots of the EKE as estimated from C_{CFB} and C_{NOCFB}, and Figure 10a depicts bivariate histogram of the same quantity. The EKE spatial patterns from C_{CFB} and C_{NOCFB} are very similar (see also Table 2), representing, for example, in the same place the eddy-rich regions such as the Western Boundary Currents. However, in agreement with previous studies, C_{NOCFB} systematically overestimates the EKE with respect to C_{CFB}. Consistently, from C_{NOCFB} to C_{CFB}, the mean and median EKE are reduced by ≈27% and 37.5%, respectively (Table 3). These reductions are much larger than the internal variability (less than 2%; see Table 3). The 95^{th} percentile roughly corresponds to Western Boundary Currents and the

Table 2
Regression (Slope and Offset) Between V_{5y} or EKE From C_{CFB} and the Other Simulations and Spatial Correlations (Excluding the Equator for the EKE)

Experiments	V_{5y}	EKE
Coupled		
C_{CFB2}	0.95; 2.0; 0.98	1.01; 0.0001; 0.97
C_{CFB3}	0.96; 1.5; 0.99	1.02; −0.0002; 0.97
C_{NOCFB}	1.00; 4.5; 0.99	1.33; 0.002; 0.94
C_{SMTH}	0.94; 3.1; 0.99	1.03; 0.0005; 0.96
Reanalysis		
$R_{NOCFB}S$	0.98; 5.3; 0.99	1.30; 0.002; 0.94
$R_{NOCFB}W_{ABS}$	0.97; 4.8; 0.99	1.30; 0.002; 0.93
$R_{CFB}W_{ABS}$	1.0; 5.2; 0.99	1.41; 0.002; 0.92
$R_{NOCFB}W_{REL}$	0.87; 1.0; 0.99	0.74; 0.0003; 0.95
$R_{CFB}W_{REL}$	0.91; 1.3; 0.99	0.82; 0.0001; 0.96
Scatterometers		
$Sc_{CFB}S$	0.96; 3.9; 0.99	1.26; 0.001; 0.93
$Sc_{CFB}W_{ABS}$	0.95; 3.7; 0.99	1.21; 0.001; 0.94
$Sc_{CFB}W_{REL}$	0.86; 1.2; 0.99	0.71; 0.0003; 0.94
Parameterized		
$R_{NOCFB}W_{REL}Ps_wC$	0.93; 0.3; 0.99	1.05; 0.0003; 0.85
$R_{NOCFB}W_{REL}Ps_wM$	0.93; 0.8; 0.99	1.07; −0.0006; 0.86
$R_{NOCFB}SPs_\tau M$	0.94; 1.7; 0.99	1.15; −0.006; 0.0.85
$R_{NOCFB}SPs_\tau P$	0.92; 2.5; 0.99	0.96; 0.0005; 0.96
$R_{CFB}SPs_\tau P$	0.93; 2.3; 0.99	0.94; 0.0005; 0.96

Agulhas Return Current, where the mean and median EKE are reduced by ≈15% and ≈20% from C_{NOCFB} to C_{CFB}, which is again larger than the internal variability of the coupled model (less than 2.2%; see Table 4).

5.3. Thermal Feedback

The mesoscale TFB causes wind and surface stress magnitude, divergence, and curl anomalies (Chelton et al., 2004, 2007; O'Neill et al., 2010, 2012; Desbiolles et al., 2016). Hogg et al. (2009), by using a "crude" parameterization of these surface stress anomalies in an idealized oceanic model, suggest that the mesoscale TFB may weaken the mean circulation by 30% to 40%. However, here, the C_{CFB_SMTH} simulation, which does not include the mesoscale SST feedback, has a mean circulation very similar to that from C_{CFB} (Figure 2a and Tables 2 and 3). Additionally, in Figure 3a, the monthly temporal evolution of V_{3m} from C_{CFB} and C_{CFB_SMTH} cannot be objectively distinguished. As shown by (Renault, Masson, et al., 2019) and illustrated in Figure 5a, C_{CFB_SMTH} has a s_τ that is very similar to that from C_{CFB}. This is explained by the fact that the surface stress anomalies induced by the mesoscale TFB are barely collocated with the surface currents. As a result, they do not systematically induce conduits of energy between the ocean and the atmosphere. In C_{CFB_SMTH} both F_eK_e and EKE in C_{SMTH} are very similar to those from C_{CFB} (Figures 7 and 9 and Tables 2, 3, and 4). While spatial differences of F_eK_e between C_{CFB} and C_{CFB_SMTH} over the whole domain are not distinguishable from differences caused by the internal variability of the model (See Figures S2b and S2d), they reveal sizable difference over Western Boundary Currents and the Agulhas Return Current that are not only due to the internal variability (see the positive values of Figures S2c and S2d). However, they remain much weaker than differences caused by the CFB. This is consistent with the fact that in C_{NOCFB}, that is, a simulation that considers only the TFB, $F_eK_e \approx 0$ (Figure 7a). Note that in C_{CFB_SMTH}, there is also a significant positive F_eK_e along the coast; however, it is not clear whether it is a filtering artifact or a real signal, but this signal is not present in, *e.g.*, $R_{NOCFB}SPs_\tau P$, which does not consider TFB either. The mesoscale TFB impact on the oceanic dynamics is beyond the scope of this study, but these first diagnostics suggest that in a forced oceanic simulation (with CFB), the lack of mesoscale TFB has a very weak effect on the mean and mesoscale oceanic circulations. Note that when large-scale gradients of SST are also smoothed (as, e.g., in Ma et al., 2016), this may impact the wind, and subsequently, the coupling coefficient s_τ (as it depends on the wind magnitude), and, finally, F_eK_e.

6. Forcing an Oceanic Model with an Atmospheric Reanalysis

In this section, the simulations forced by a synthetic reanalysis product (Table 1), namely, $R_{NOCFB}S$, $R_{NOCFB}W_{ABS}$, $R_{CFB}W_{ABS}$, $R_{NOCFB}W_{REL}$, and $R_{CFB}W_{REL}$) are compared to C_{CFB}. The aim of this section is to assess the biases caused by forcing an oceanic simulation with an atmospheric reanalysis in terms of mean circulation, coupling coefficient between the mesoscale surface currents vorticity and stress curl, sinks of energy, and mesoscale activity. Table 2 details the regressions of V_{5y} and EKE from C_{CFB} and the Reanalysis-like simulations. In all the forced simulations, both V_{5y} and EKE have a spatial pattern similar to those from C_{CFB} (see also Figure 10 for the EKE). Tables 3 and 4 provide some mean and median values of V_{5y}, F_eK_e, and EKE.

6.1. Large Scale

Figure 2c shows the box plots of V_{5y} as estimated from $R_{NOCFB}S$, $R_{NOCFB}W_{ABS}$, $R_{CFB}W_{ABS}$, $R_{NOCFB}W_{REL}$, and $R_{CFB}W_{REL}$. Not surprisingly, two kind of simulations can be distinguished: the simulations forced with or without CFB. Consistent with the previous section, the oceanic simulations $R_{NOCFB}S$, $R_{NOCFB}W_{ABS}$, $R_{CFB}W_{ABS}$, which ignore the CFB when estimating the surface stress, overestimate the mean and median of V_{5y} by at least 5.5% (and up to 11.5%; which is larger than the internal variability, see also Table 3). In that sense, they are very similar to C_{NOCFB} (see Figure 2b and Table 3). By contrast, the simulations $R_{NOCFB}W_{REL}$ and $R_{CFB}W_{REL}$, which take into account the CFB when estimating the surface stress, underestimate V_{5y} mean

Table 3
Mean and Median of V_{5y}, F_eK_e, and EKE Over the Whole Domain (Excluding the Equator for F_eK_e and EKE and, for F_eK_e, Excluding the Signal Along the Coast That Is Not Caused by CFB) for the Coupled Simulations and the Forced Simulations

Experiments	V_{5y} [m^2 s^{-1}]	F_eK_e [10^{-7} m^3 s^{-3}]	EKE [cm^{2}s^{-2}]
Coupled			
C_{CFB}	39.2; 17.1	−3.9; −1.3	165; 75
C_{CFB2}	39.0; 17.2	−3.9; −1.2	162; 74
C_{CFB3}	39.6; 17.2	−4.0; −1.4	168; 81
C_{NOCFB}	42.3; 18.6	−0.17; 0.1	225; 120
C_{SMTH}	39.0; 17.1	−4.2; -1.4	175; 81
Reanalysis			
$R_{NOCFB}S$	42.1; 18.6	−0.1; 0.1	228; 123
$R_{NOCFB}W_{ABS}$	41.5; 18.3	−0.1; 0.1	222; 116
$R_{CFB}W_{ABS}$	42.9; 19.1	0.2; 0.2	243; 132
$R_{NOCFB}W_{REL}$	36.0; 15.8	−5.2; −1.5	133; 53
$R_{CFB}W_{REL}$	37.1; 16.5	−5.3; −1.5	145; 61
Scatterometers			
$Sc_{CFB}S$	40.6; 18.2	−0.3; −0.1	215; 112
$Sc_{CFB}W_{ABS}$	40.3; 17.7	−0.3; 0.0	209; 108
$Sc_{CFB}W_{REL}$	35.5; 15.6	−5.5; −1.5	126; 51
Parameterized			
$R_{NOCFB}W_{REL}Ps_wC$	37.8; 16.3	−4.1; −1.2	174; 68
$R_{NOCFB}W_{REL}Ps_wM$	37.9; 16.3	−3.9; −1.1	179; 73
$R_{NOCFB}SPs_\tau M$	38.6; 16.8	−3.7; −1.1	188; 76
$R_{NOCFB}SPs_\tau P$	38.1; 16.9	−4.0; −1.2	162; 71
$R_{CFB}SPs_\tau P$	38.8; 17.2	−4.1; −1.2	166; 73

(median) by 8.2% and 5.3% (7.6% and 3.5%), respectively, again larger than the differences between C_{CFB} and the perturbed coupled simulations (Table 3). This underestimation is explained by the fact that these simulations lack or partially lack a coherent wind response to CFB, which should partly re-energize the mean currents (Renault, Molemaker, McWilliams, et al., 2016). Figure 3b represents the monthly evolution of V_{3m}. Consistent with the previous results, after about a year, the first/main temporal adjustment (i.e., a large increase of V_{3m}) of the mean circulation is achieved, and the differences between the experiments are robust and clearly visible. It is worth noting that the atmospheric forcing derived from C_{CFB} already contains a mean wind response that is coherent with the C_{CFB} mean surface currents. As a consequence, the mean winds used to force $R_{CFB}W_{ABS}$ ($R_{CFB}W_{REL}$) are slightly re-energized in comparison with the forcing used in $R_{NOCFB}W_{ABS}$ ($R_{NOCFB}W_{REL}$). V_{3m} in $R_{CFB}W_{ABS}$ ($R_{CFB}W_{REL}$) is then larger than in $R_{NOCFB}W_{ABS}$ ($R_{NOCFB}W_{REL}$, Figure 3b). The mean oceanic circulation over the 5-year period considered here is not fully deterministic. As a result, the imprint of the C_{CFB} mean surface current on the wind is not fully coherent with those from the forced simulations and none of the forced simulations reproduce the correct value of V_{3m}. This has an important consequence, as it means that a wind and stress that have an imprint of the surface currents cannot be directly used with a parameterization of the CFB. As discussed in Section 9, they should be first corrected for the influence of the currents on the reanalysis.

6.2. Mesoscale

At the mesoscale, again, the simulations forced with and without CFB can be distinguished. On the one hand, the simulations forced without CFB behave in a very similar way as C_{NOCFB}: The resulting stress does not have the imprint of the simulated mesoscale eddies and, thus, does not have any mesoscale correlation with them. As a result, $s_\tau \approx 0$, $F_eK_e \approx 0$, and global mean and median of the EKE is overestimated by at least 34% and 54%, respectively, compared with C_{CFB} (Figures 4, 5b, 6, 7b, 8, and 9b and Table 3). Consistent with the literature, oceanic simulations forced without CFB overestimate not only the mean circulation but also the mesoscale activity. This overestimation is confirmed by estimating bivariate histogram between, for

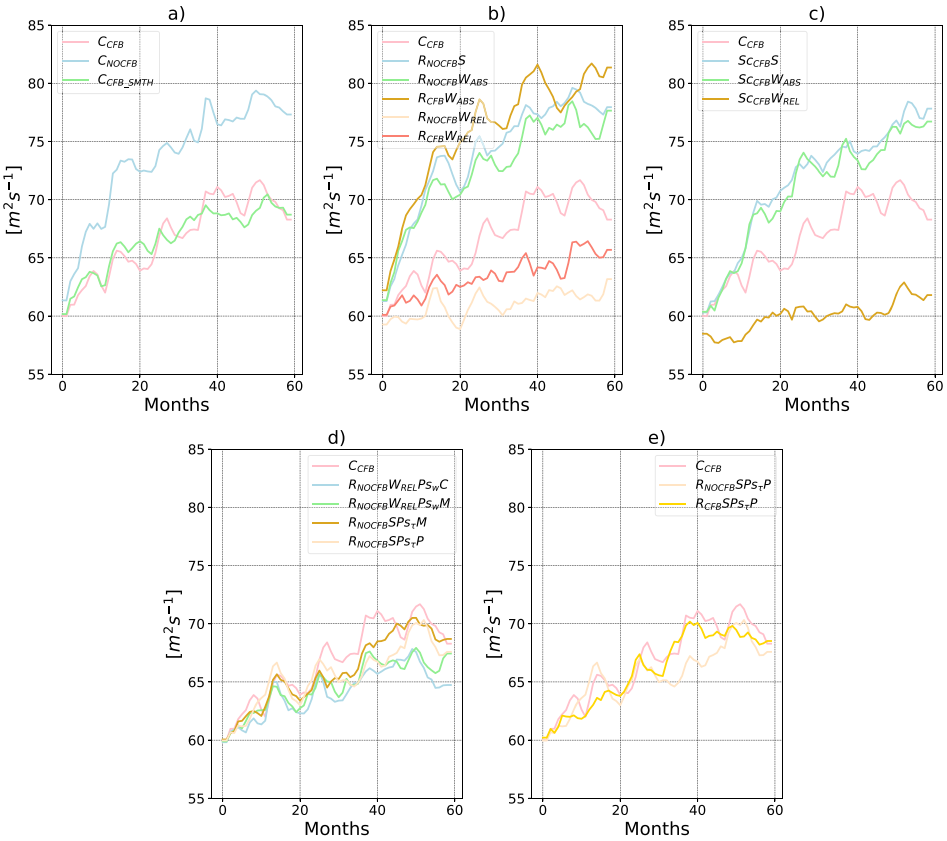

Figure 3. Monthly evolution of V_{3m} (m^2 s^{-1}) as simulated by the coupled and forced simulations and averaged over the whole domain.

example, $R_{NOCFB}W_{ABS}$ and C_{CFB} (Figure 10b; similar results are found for the other experiments of the same kind). As C_{NOCFB}, the forced simulations that ignore the CFB largely overestimate the EKE. On the other hand, the simulations forced with CFB, that is, $R_{NOCFB}W_{REL}$ and $R_{CFB}W_{REL}$, have an opposite behavior. As illustrated in Figure 5b, in this simulation, s_τ is overestimated (i.e., too negative) in term of mean, median, quartiles, and 95^{th} percentile by roughly 30%, which is consistent with (Renault, Molemaker, McWilliams, et al., 2016). Note that when the wind is derived from C_{CFB}, it already contains the mesoscale wind response to the mesoscale eddies simulated by C_{CFB}. Even if $R_{CFB}W_{REL}$ is forced by the C_{CFB} winds and uses the same initial conditions, $R_{CFB}W_{REL}$ and C_{CFB} eddies become uncorrelated after a few months. Therefore, the C_{CFB} mesoscale wind anomalies do not properly counteract the surface stress response to the CFB and $R_{CFB}W_{REL}$ and $R_{NOCFB}W_{REL}$ have a very similar s_τ (Figure 5b). The systematic underestimation of the EKE is also confirmed by the bivariate histogram between, for example, $R_{NOCFB}W_{REL}$ and C_{CFB} shown in Figure 10c.

s_τ can be interpreted as a measure of the efficiency of the eddy killing. This is corroborated by Figure 6b that shows the spatial distribution of F_eK_e as estimated from $R_{CFB}W_{REL}$ (similar results are found using $R_{NOCFB}W_{REL}$) and by Figure 7b that depicts the F_eK_e box plots for these simulations (see also Table 3). When taking into account the CFB, the global mean (median) sinks of energy are overestimated by at least 33% (15%) with respect to C_{CFB}. The most striking features are situated over the Western Boundary Currents (the 5^{th} percentile of the F_eK_e and 95^{th} percentile of the EKE), where the sinks of energy are clearly more intense in $R_{CFB}W_{REL}$ and $R_{NOCFB}W_{REL}$ than C_{CFB} (see also Table 4). As expected, these sinks of energy cause excessive damping of the mesoscale activity everywhere with respect to C_{CFB}, which is much larger than the internal variability of the coupled model (Figures 8a, 8c, and 9b and Tables 3 and 4). This is also consistent with the results of (Renault, Molemaker, McWilliams, et al., 2016) for the California region.

To conclude this section, when using a reanalysis or a coupled simulation like C_{NOCFB} to force an ocean model, at the large scale, neglecting the CFB leads to an overestimation of the mean oceanic circulation strength. However, when taking into account the CFB by using the relative wind to the oceanic motions in

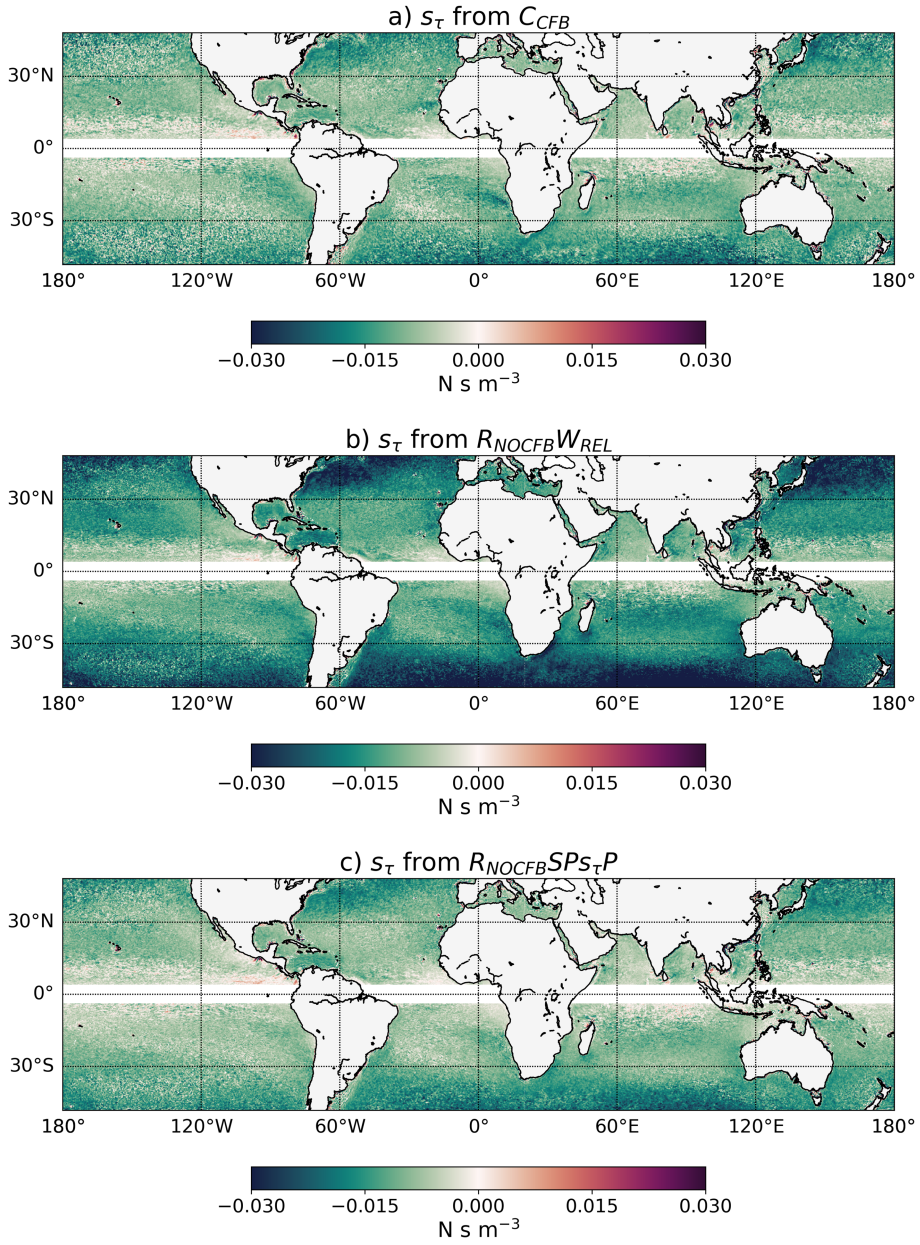

Figure 4. Coupling coefficient between the mesoscale geostrophic surface current vorticity and the surface stress curl (s_τ) as estimated from (a) C_{CFB}, (b) $R_{NOCFB}W_{REL}$, and (c) $R_{NOCFB}SPs_\tau P$. The Equator is excluded because of the geostrophic approximation.

the surface stress estimation, the mean circulation becomes too weak. At the mesoscale, as expected, when ignoring the CFB (by using a prescribed surface stress or an absolute wind), the sinks of energy induced by the CFB are not reproduced, and the EKE is significantly overestimated. By contrast, the use of the wind relative to the oceanic motions causes an overestimation of s_τ and F_eK_e and, thus, of the damping of the mesoscale activity with respect to C_{CFB}. The prescribed wind does not have a coherent response to the simulated oceanic currents and, thus, does not partially re-energize the mesoscale activity. Note that because the same bulk formulae are used in both WRF and NEMO, the estimated surface stress in WRF is similar to the estimated surface stress in NEMO. As a result, the forced oceanic simulations without CFB are very close to C_{NOCFB}. Forcing an oceanic model with a forcing derived from a reanalysis-like product (with or without CFB) and without a proper parameterization of the CFB is not suitable. However, as discussed in Section 8, such products can be used with a parameterization of the CFB.

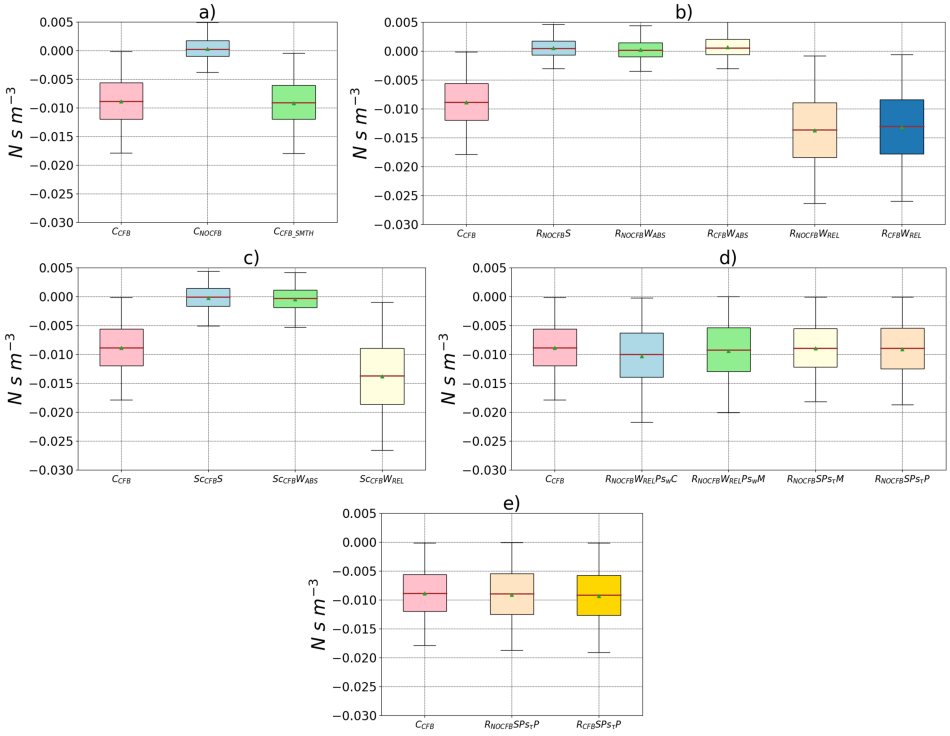

Figure 5. Box plots as described in Figure 2 but for the spatial variability of s_τ as estimated from (a) C_{CFB}, (b) the reanalysis-like simulations, (c) the scatterometer-like simulations, (d) the parameterized simulations, and (e) the parameterized simulations $R_{NOCFB}SPs_\tau P$ and $R_{CFB}SPs_\tau P$. The box plot of s_τ estimated from C_{CFB} is shown in all the box plots for clarity.

7. Forcing an Oceanic Model with Scatterometer Winds or Stress

In this section, the simulations $Sc_{CFB}S$, $Sc_{CFB}W_{ABS}$, and $Sc_{CFB}W_{REL}$ are compared to C_{CFB}. The goal of this section is to quantify the biases induced by forcing an oceanic simulation with scatterometer stress or wind in terms of V_{5y}, V_{3m}, s_τ, the sink of energy, and mesoscale activity. Again, as revealed by Table 2, in all the forced simulations, both V_{5y} and EKE have a spatial pattern similar to those from C_{CFB}. Tables 3 and 4 provide statistics comparison to other simulations.

7.1. Large Scale

As for the reanalysis forcing, the simulations forced with absolute wind or stress (i.e., without CFB: $Sc_{CFB}S$ and $Sc_{CFB}W_{ABS}$) and with relative wind (i.e., with CFB: $Sc_{CFB}W_{REL}$) clearly differ from the others. Figure 2c shows box plots of V_{5y} as estimated from C_{CFB} and these simulations. When forcing an ocean model with scatterometer stress or absolute wind, the global mean of V_{5y} is overestimated with respect to C_{CFB}, but only by ≈3%, that is, less than the overestimation observed in C_{NOCFB} but still larger than the internal variability of the coupled model (Table 3). Two main factors can explain such a difference. On one hand, the mean stress and wind used here are derived from C_{CFB} in order to mimic scatterometers; that is, the stress has the imprint of the mean surface currents, and the wind is relative to the mean C_{CFB} surface currents. If the mean surface currents from C_{CFB} were identical to those in $Sc_{CFB}S$ or $Sc_{CFB}W_{ABS}$, the CFB effect on the large scale would be correctly reproduced when forcing an ocean model with scatterometer data. On the other hand, over the 5-year period considered here, the large-scale currents are only partially deterministic. Therefore, although similar, the mean surface currents in these three scatterometer-like simulations are not identical to that from C_{CFB}. As a result, when forcing an ocean model with a scatterometer-like forcing, the CFB slowdown of the mean circulation is only partly reproduced with respect to that simulated by C_{CFB}. By contrast, when using the relative wind on top of scatterometer-like winds ($Sc_{CFB}W_{REL}$), the effect of the CFB on the surface stress is potentially doubly accounted for (not exactly as the mean currents are not totally deterministic). Subsequently, the slowdown effect is overestimated, resulting in an underestimation of V_{5y} by ≈6.5% with respect to C_{CFB}; that is, in $Sc_{CFB}W_{REL}$, V_{5y} is weaker than that from $R_{CFB}W_{REL}$ (Table 3). Similar results are found when assessing V_{3m} (Figure 3c). To sum up, from a large-scale circulation perspective, the relative

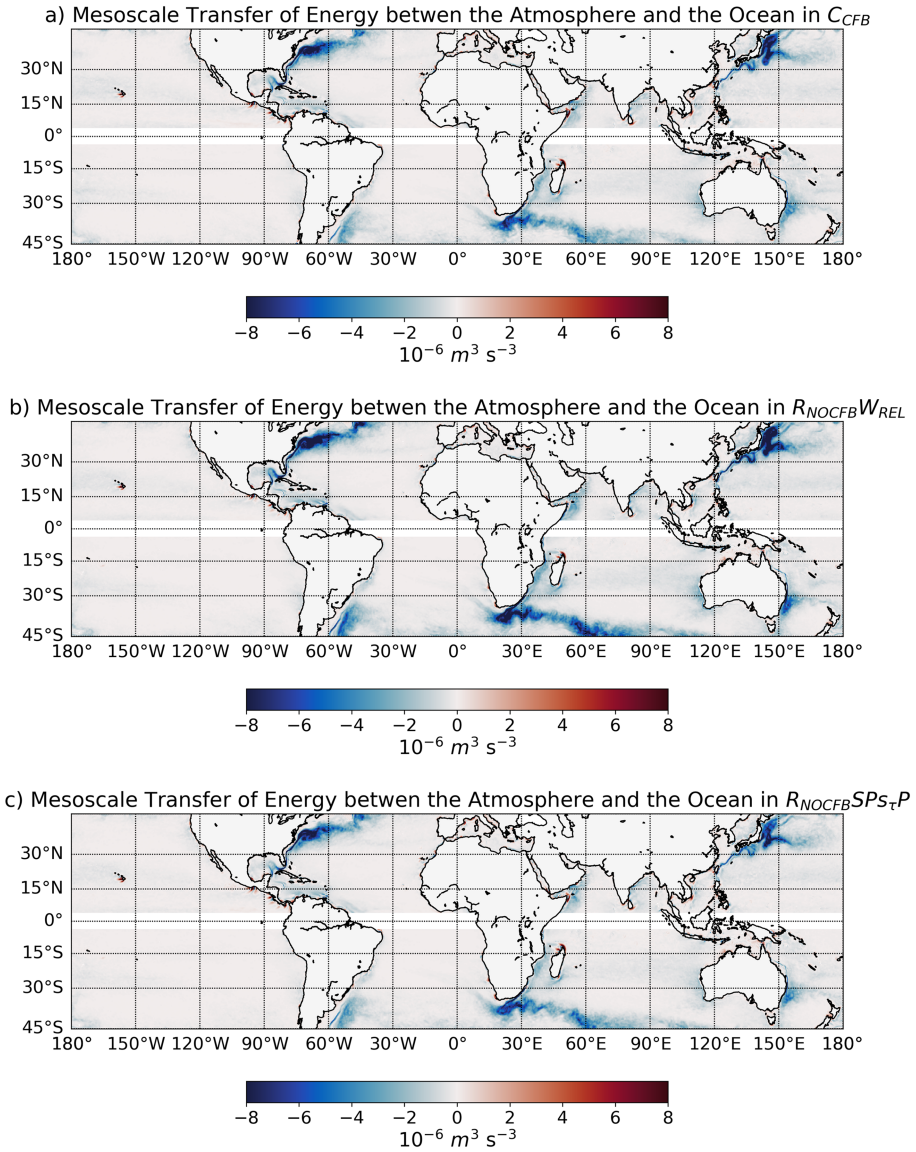

Figure 6. Mesoscale transfer of energy between the ocean and the atmosphere (F_eK_e) from (a) C_{CFB}, (b) $R_{NOCFB}W_{REL}$, and (c) $R_{NOCFB}SPs_{\tau}P$. The Equator is excluded because of the geostrophic approximation. A negative value indicates a transfer of energy from the Ocean to the atmosphere.

wind cannot be used on top of scatterometer wind as the wind (and stress) already contains the surface stress response responsible of the slow down of the mean circulation.

7.2. Mesoscale

As explained in Section 6, at the mesoscale, as for a simulation forced by a reanalysis, neither $Sc_{CFB}S$ nor $Sc_{CFB}W_{ABS}$ can dampen the mesoscale activity as the CFB mesoscale surface stress anomalies present in the prescribed surface stress are not correlated with the eddies simulated by the forced simulations. In both simulations, as illustrated in Figures 5c, 7c, and 9c, and Tables 3 and 4, $s_{\tau} \approx 0$, $F_eK_e \approx 0$, and the EKE is overestimated by ≈27% with respect to C_{CFB}, which is again much larger than the internal variability (Table 3). The bivariate histograms of the EKE between C_{CFB} and $Sc_{CFB}S$ ($Sc_{CFB}W_{ABS}$) are x similar to that between C_{CFB} and C_{NOCFB} (not shown). When taking into account the CFB by using the relative wind instead of the absolute wind ($Sc_{CFB}W_{REL}$), again because the simulated eddies are not correlated with the prescribed wind, s_{τ} is overestimated (i.e., too negative), F_eK_e is too large, and the EKE too weak (in both mean and median, again with differences larger than those cause by the internal variability of the coupled model). Not

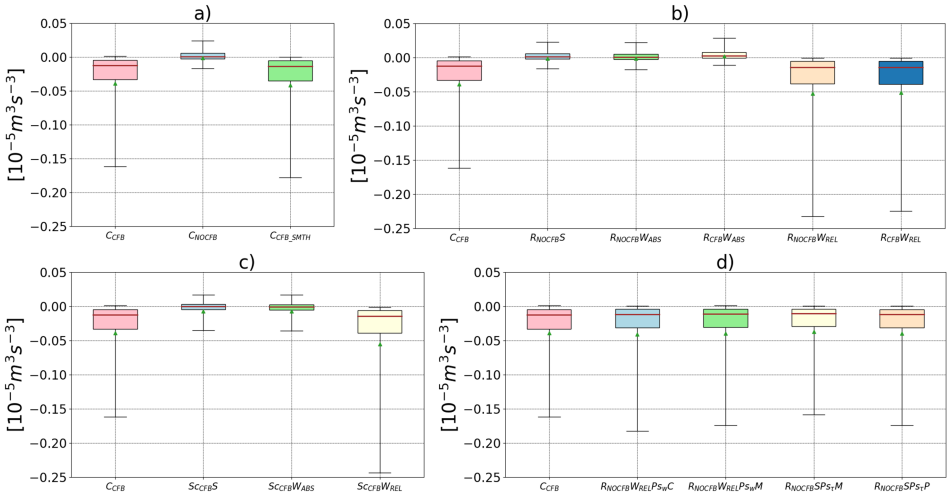

Figure 7. Same as Figure 5 but for the F_eK_e.

surprising, the bivariate histogram of the EKE between C_{CFB} and $Sc_{CFB}W_{REL}$ is very similar to that between C_{CFB} and $R_{NOCFB}W_{REL}$.

These results on the large scale and on the mesoscale have an important consequence on how to force an oceanic model. Wind or stress forcing derived from scatterometer data may reproduce relatively realistically the mean CFB effect on the large-scale circulation but not the eddy killing effect. It also means that a parameterization of the wind response cannot be used directly on top of a scatterometer forcing as, although it may reproduce the mesoscale effect (see Section 8), it would overestimate the CFB large-scale effect and, thus, the slowdown of the mean circulation. Similar results are found when forcing the oceanic model with wind or the stress.

Table 4
Mean and Median of the F_eK_e and the EKE Over Western Boundary Currents and the Agulhas Return Current, Identified as the Regions With a F_eK_e More Negative Than the 5th Percentile or an EKE Larger Than the 95th Percentile for the Coupled Simulations and the Forced Simulations

Experiments	F_eK_e [10^{-7} m^3 s^{-3}]	EKE [cm^{2}s^{-2}]
Coupled		
C_{CFB}	−37.7; −26.8	1,237; 960
C_{CFB2}	−37.2; −26.5	1,223; 957
C_{CFB3}	−37.1; −27.3	1,210; 958
C_{NOCFB}	−9.1; −3.0	1,450; 1,190
C_{SMTH}	−38.8; −29.5	1,292; 1,029
$R_{NOCFB}S$	−9.1; −3.1	1,481; 1,211
Reanalysis		
$R_{NOCFB}W_{ABS}$	−8.1; −3.3	1,463; 1,173
$R_{CFB}W_{ABS}$	−6.8; −2.1	1,555; 1,270
$R_{NOCFB}W_{REL}$	−53.1; −40.1	1,077; 838
$R_{CFB}W_{REL}$	−51.4; −39.4	1,140; 896
Scatterometers		
$Sc_{CFB}S$	−14.1; −6.5	1,411; 1,153
$Sc_{CFB}W_{ABS}$	−13.5; −6.7	1,389; 1,126
$Sc_{CFB}W_{REL}$	−55.8; −42.1	1,029; 794
Parameterized		
$R_{NOCFB}W_{REL}Ps_wC$	−40.5; −30.6	1,369; 1,088
$R_{NOCFB}W_{REL}Ps_wM$	−38.9; −28.4	1,385; 1,097
$R_{NOCFB}SPs_\tau M$	−35.7; −25.8	1,439; 1,150
$R_{NOCFB}SPs_\tau P$	−38.6; −28.8	1,231; 977
$R_{CFB}SPs_\tau P$	−39.9; −29.4	1,260; 996

8. Parameterizing the CFB in a Forced Oceanic Model

As demonstrated in the previous sections, an oceanic simulation should have a parameterization of the CFB in order to have a realistic representation of the oceanic mean and mesoscale circulations. Because of the absence of a current imprint on the wind or stress, wind reanalyses without CFB are the simplest choice (together with atmospheric uncoupled or coupled models without CFB) when combined with a parameterization of the wind response to the CFB. As described in Section 3, four additional simulations based on reanalysis-like wind (Table 1), namely, $R_{NOCFB}W_{REL}Ps_wC$, $R_{NOCFB}W_{REL}Ps_wM$, $R_{NOCFB}SPs_\tau M$, and $R_{NOCFB}SPs_\tau P$) are carried out to test different kinds of parameterization of the CFB. As for the other forced simulations, in all the parameterized simulations, V_{5y} and EKE have a similar spatial pattern to those from C_{CFB} (see Table 2 and bivariate histograms in Figure 10defg). Additionally, Tables 3 and 4 summarize the mean and median quantities of V_{5y}, F_eK_e, and EKE estimated from these simulations at a quasi-global scale and over the Western Boundary Currents and the Agulhas Return Current.

8.1. Large Scale

The box plots of V_{5y} as estimated from C_{CFB} and the parameterized simulations are illustrated in Figure 2e. Figure 3b represents the monthly evolution of V_{3m}. All the parameterized simulations correctly reproduce the characteristics of V_{5y} as simulated by C_{CFB}, although, on average, they have a weak underestimation of mean and median by less than 3%. The temporal evolution of V_{3m} is also fairly well reproduced in all the simulations. Although more years of simulations should be used to draw a more robust conclusion,

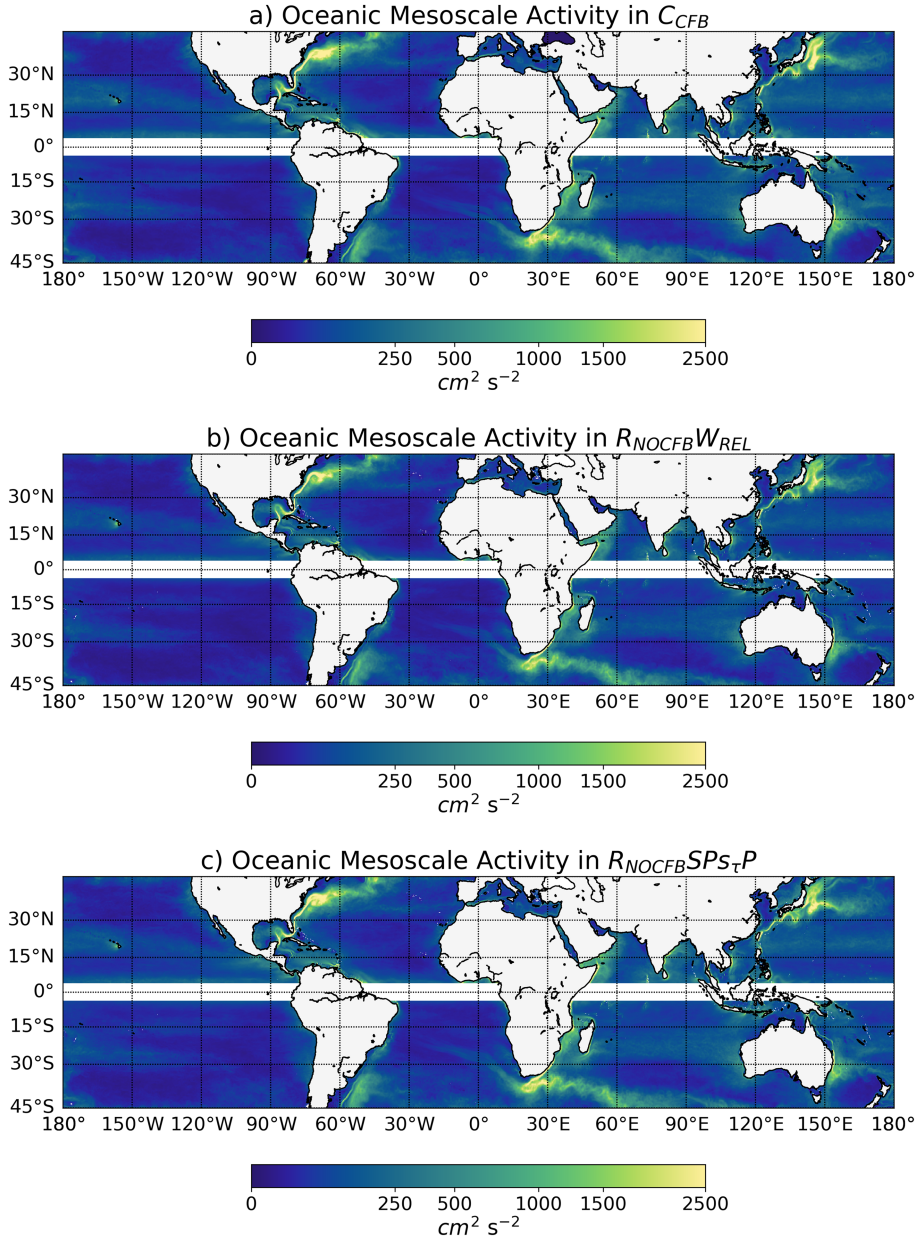

Figure 8. Eddy Kinetic Energy (EKE) from (a) C_{CFB}, (b) $R_{NOCFB}W_{REL}$, and (c) $R_{NOCFB}SPs_{\tau}P$. The equator is excluded because of the geostrophic approximation. The sinks of energy induced by the CFB are responsible of an "eddy killing", that is, a damping of the mesoscale activity.

a simulation with a parameterization based on s_{τ} is closer to C_{CFB} than a simulation with a parameterization based on s_w (see also Table 3 and 4).

8.2. Mesoscale

Figures 5d, 7d, and 9d represent the box plots of s_{τ}, F_eK_e, and EKE from C_{CFB} and from the four parameterized simulations. Tables 3 and 4 provide the mean and median of the F_eK_e and EKE estimated over the whole domain and over the Western Boundary Currents, respectively. To first order, all the parameterizations improve the realism of the simulation in terms of s_{τ}, F_eK_e, and EKE with respect to a classic forced simulation with (or without) CFB (see previous section). The representation of the mean, median, quartiles, and 5^{th} or 95^{th} percentile (i.e., the Western Boundary Currents and the Agulhas Return Current) of these variables are clearly improved.

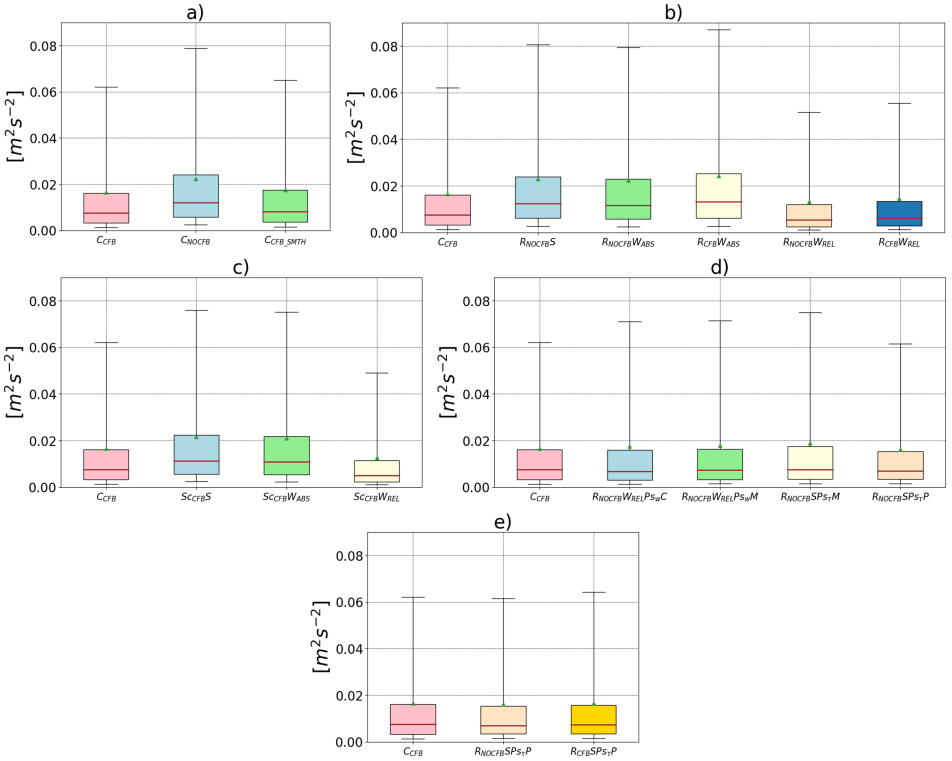

Figure 9. Same as Figure 5 but for the EKE.

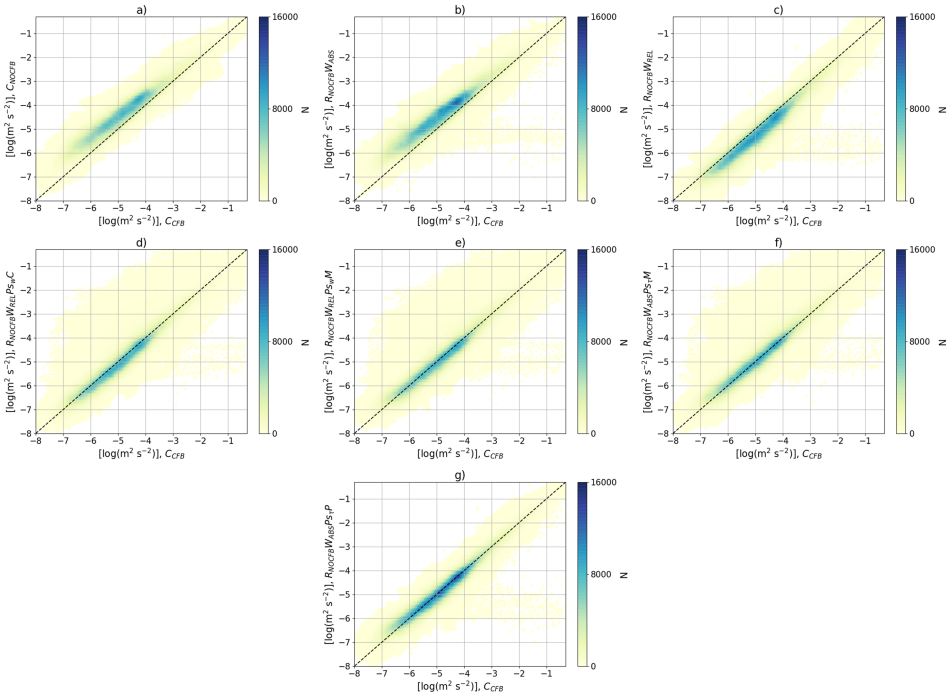

Figure 10. Bivariate histograms comparing the logarithm of the EKE from C_{CFB} to other experiments. N represents the number of occurrence.

8.3. Best Parameterization

The parameterizations based on s_τ lead in general to slightly more realistic results. This is likely because (i) the estimation of s_τ suffers from less uncertainties than the estimation of s_w because the stress response to the CFB is relatively larger than the subsequent wind adjustment and, thus, easier to properly isolate (Renault, Molemaker, McWilliams, et al., 2016) and (ii) because of the quadratic nature of the stress in the bulk formula, the error and uncertainties related to s_w are amplified. As a result, the scatterplot between wind curl and current vorticity has a larger spread than that between stress curl and current vorticity (see Figures 8 and 10 of (Renault, Molemaker, McWilliams, et al., 2016), which may tend to underestimate s_w and the partial re-energization of the large-scale circulation.

However, at the mesoscale, there is an apparent contradiction. On one hand, s_τ and F_eK_e are better represented in s_τ-based parameterizations with respect to s_w ones. On the other hand, as shown in Figure 9d, in $R_{NOCFB}W_{REL}Ps_wC$, $R_{NOCFB}W_{REL}Ps_wM$, and $R_{NOCFB}SPs_\tau M$, although the sink of energy is either well represented (mean and median) or slightly too large (e.g., in the 5^{th} percentile), the EKE is too intense both in terms of global means/medians and also over the Western Boundary Currents and the Agulhas Return Current. By contrast, in $R_{NOCFB}SPs_\tau P$, where s_τ is predicted by the wind, the F_eK_e and the EKE are fairly well represented everywhere, including over the Western Boundary Currents and the Agulhas Return Current. We hypothesize that this counterintuitive result might be explained by nonlinearities in the ocean and during a typical eddy life, as follows: Over an eddy, the use of a constant or statistical s_w or s_τ does not allow representation of high-frequency large sinks of energy that happen in the presence of an intense wind burst: The more intense the wind, the larger the sink of energy (Renault, McWilliams, & Masson, 2017). Those large and brief sinks of energy can destabilize an eddy and, thus, diminish its lifetime. Over the lifetime of an eddy, the high-frequency variations of s_τ (represented in C_{CFB} and in $R_{NOCFB}SPs_\tau P$) weakens the transfer of energy from the ocean to the atmosphere while enhancing the dissipation of the eddy energy in the ocean. These high-frequency variations of s_τ and F_eK_e are not represented in $R_{NOCFB}W_{REL}Ps_wC$, $R_{NOCFB}W_{REL}Ps_wM$, nor $R_{NOCFB}SPs_\tau M$. Indeed, in these simulations, over an eddy, the sink of energy is either constant or it represents the climatological variations of s_τ, slowly diminishing the eddy energy. This effect can be interpreted as an efficiency of the destabilization of an eddy: s_τ in $R_{NOCFB}SPs_\tau P$ (varying as a function of U_{10abs}) may be more efficient in destabilizing an eddy than in the other parameterized simulations. This conjecture requires further investigation. The better behavior of $R_{NOCFB}SPs_\tau P$ in representing the EKE is also confirmed by analyzing the bivariate histograms between the EKE from C_{CFB} and the parameterized experiments (Fig. 10). All the parameterizations improve the represention of the EKE compared to the other forced simulations. However, as revealed by Figure 10g, a parameterization based on a predicted s_τ reduces the spread of the bivariate histogram and allows a better representation of the EKE over its entire energetic range. The remaining scattering in Figure 10g is mainly due to the chaotic nature of EKE as the bivariate histogram between C_{CFB} and $R_{NOCFB}SPs_\tau P$ is very similar to that between C_{CFB} and *e.g.,* C_{CFB2} (see the supporting information).

Using a predicted s_τ (as in $R_{NOCFB}SPs_\tau P$) appears therefore as the best strategy to force an ocean model as it allows to better mimic the behavior of a coupled model, representing more physics and more processes than parameterizations based on simple constant coupling coefficients. Note that these differences among the simulations are even more present over the Western Boundary Currents, that is, over the most eddying region of the world. Figures 4c, 6c, and 8c illustrate the spatial distribution of the mean s_τ, F_eK_e, and EKE as estimated from $R_{NOCFB}SPs_\tau P$. They can be compared to C_{CFB} and $R_{NOCFB}W_{REL}$ (i.e., a simulation forced with a relative wind but without a parameterization) from which the same quantities are represented on the same Figures. Consistent with the box plot analysis, $R_{NOCFB}SPs_\tau P$ is very similar to C_{CFB} and allows us to overcome the overestimation of those quantities when forcing an oceanic model with a relative wind. In addition, as shown in Section 9, another advantage of $R_{NOCFB}SPs_\tau P$ lies in the fact that it can be used on top of a prescribed surface stress or an estimated surface stress. Finally, discrepancies observed between the parameterized simulations and C_{CFB} especially over the Western Boundary Currents can also originate from a slightly different generation of mesoscale activity by baroclinic and barotropic instabilities (Renault, McWilliams, & Penven, 2017). However, this would have a second-order effect on the EKE with respect to the sinks of energy as the ensemble simulations of C_{CFB} give very close results in terms of F_eK_e and EKE C_{CFB}.

9. Forcing an Oceanic Model with Future Reanalysis

Global models (reanalysis and climate models) are already or will inevitably take into account the CFB. This is, for example, the case of the latest ECMWF (European Center Medium Weather Forecast) reanalysis.

Paradoxically, this could be problematic from an oceanic modeling forcing perspective. As for a scatterometer, the CFB effects on the stress and wind would have already been included in the wind and surface stress derived from the reanalysis. Forcing an oceanic model with this kind of atmospheric forcing, would result in lower quality of the representation of the deterministic currents (see Section 7). Usually, reanalysis products provide the surface stress and a diagnosed wind at 10 m, which is, if the CFB is accounted for, relative to the surface currents ($\boldsymbol{U_{10rel}}$ see sections 2). Note that in this case $\boldsymbol{U_{10rel}}$ already contains the wind response to the CFB. If using $\boldsymbol{U_{10rel}}$, the surface stress should first be estimated as usual: $\boldsymbol{\tau_{rea}} = \rho_a C_D |\boldsymbol{U_{10rel}}| \boldsymbol{U_{10rel}}$. Then, the estimated or provided surface stress ($\boldsymbol{\tau_{rea}}$) should be corrected by removing the influence of the reanalysis surface currents ($\boldsymbol{U_{orea}}$) and then by adding up that from the simulated surface currents ($\boldsymbol{U_o}$), following:

$$\boldsymbol{\tau} = \boldsymbol{\tau_{rea}} + s_\tau \quad (\boldsymbol{U_o} - \boldsymbol{U_{orea}}). \tag{11}$$

If $\boldsymbol{U_{10rel}}$ is provided, then the surface stress should be estimated following:

$$\boldsymbol{\tau} = \rho_a C_D |\boldsymbol{U_{10rel}}| (\boldsymbol{U_{10rel}}) + s_\tau \quad (\boldsymbol{U_o} - \boldsymbol{U_{orea}}). \tag{12}$$

This procedure should allow the removal of the wind and stress anomalies induced by the oceanic surface currents of the reanalysis and replacing them with those induced by the simulated currents of the oceanic simulation. To test this strategy, a final forced oceanic simulation ($R_{CFB}SPs_\tau P$) is carried out using the surface stress and oceanic surface currents from C_{CFB} and applying equation (11). Figures 2f, 3e, 5e, and 9e and Tables 4, 3, and 2 show the main results at both the large-scale and the mesoscale. In $R_{CFB}SPs_\tau P$ the spatial distribution and statistics of both V_{5y} and V_{3m} are very similar to the ones simulated by C_{CFB} and $R_{NOCFB}SPs_\tau P$. This indicates that although the stress from the reanalysis already contains the effect of the mean currents, the stress correction (11) allows us to efficiently remove the large-scale CFB imprint of the reanalysis stress and to replace it by one that is coherent with the simulation.

At the mesoscale in $R_{CFB}SPs_\tau P$, the reanalysis eddy imprint on the stress (wind) is also removed by using (11). However, because the eddies of the reanalysis are not in the same place as they are in $R_{CFB}SPs_\tau P$, even without correcting the surface stress, the mesoscale CFB effect should be correctly represented compared to C_{CFB}. This is confirmed by Figure 9f and Tables 3 and 4. In $R_{CFB}SPs_\tau P\, s_\tau$, the sinks of energy and the EKE are also very similar to the ones simulated by C_{CFB} and $R_{NOCFB}SPs_\tau P$. To conclude, in the coming years, such a strategy could be easily applied; however, a *sine qua non* condition is that the atmospheric fields are provided along with the corresponding oceanic surface currents. A similar strategy could be applied to scatterometer data, but in this case, a coherent surface current measure should be provided (which is not possible yet with the existing satellites).

10. Summary and Discussion

Several recent studies demonstrate the importance of taking into account the effect of the surface oceanic current on the stress and on the wind (CFB) in order to realistically reproduce the oceanic mean circulation and mesoscale activity. These past studies raise the important question of how to best to force an oceanic model. In this study, using a realistic tropical channel (45°S to 45°N) domain for ocean-atmosphere coupled and uncoupled oceanic simulations, we assess to what extent a forced oceanic simulation can reproduce the mean oceanic circulation, the coupling coefficient between the surface oceanic currents and stress, the sinks of energy induced by the CFB, and the mesoscale activity compared to a coupled simulation that includes CFB.

Consistent with previous studies, we first confirm that the CFB slows down the mean circulation and dampens the mesoscale activity. We then assess to what extent an oceanic simulation can be forced by wind or stress as derived from an atmospheric reanalysis or scatterometer products such as QuikSCAT. Figure 11 shows a sketch that sums up the following. Three kinds of forced simulations are distinguished depending on the source of the wind or stress forcing: The wind (stress) can be derived from (1) a reanalysis that did not feel the CFB (labeled a–d, in Figure 11), (2) a reanalysis in which the CFB is accounted for (labeled e–i in Figure 11), and (3) a scatterometer. When using a wind from a reanalysis forcing product that does not include CFB, the forced simulations that use an absolute wind or a prescribed surface stress overestimate the mean circulation strength and the mesoscale activity with respect to a coupled simulation with CFB (a in

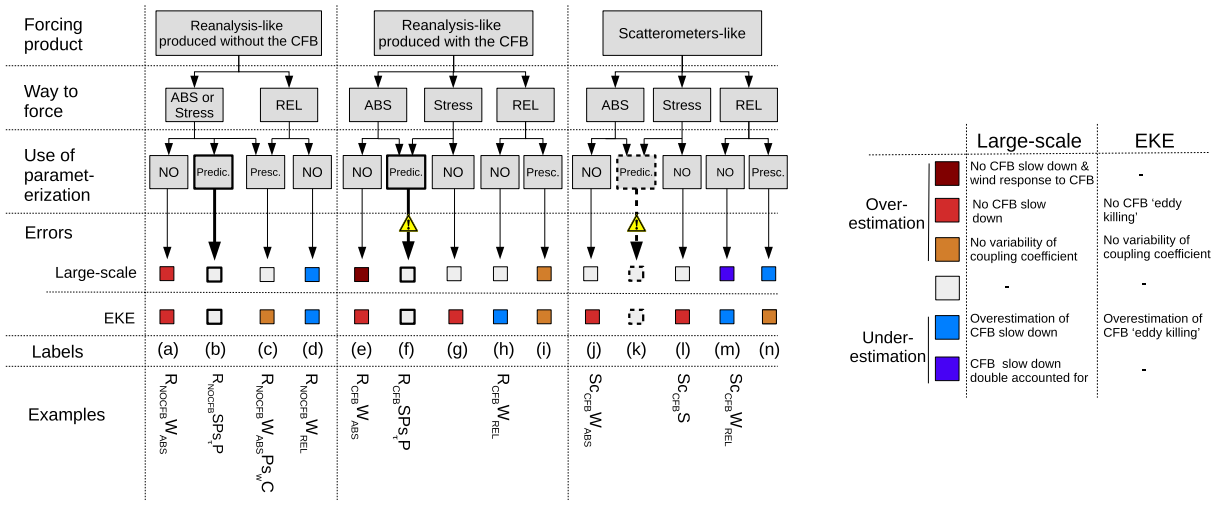

Figure 11. How to best force an oceanic model? This sketch sums up the main methods. In order to illustrate the possible error made by the different strategies, two main indicators are used: the large-scale circulation and the mesoscale circulation. A blue color indicates an underestimation, the reddish colors gradually highlight an overestimation, and the white color means that the circulation is roughly correctly represented. "Presc." stands for a prescribed coupling coefficient (s_w or s_τ) and "Predic." for a predicted one (s_τ). The warning sign indicates that coherent surface currents with the atmospheric forcing from the reanalysis-like or from the observations are needed. Such a product is not yet available for the observations (dashed lines). Best way to force an oceanic model is highlighted with bold lines.

Figure 11). By contrast, when using the relative wind, they overestimate the slowdown of the mean circulation and the damping of the mesoscale activity induced by the CFB because of their lack of a wind response (d in Figure 11). If the reanalysis previously felt the CFB, because of the already accounted for presence of the large-scale wind response to the CFB, an absolute wind forcing will result in a large overestimation of the mean circulation strength (e in Figure 11) and in an overestimation of the mesoscale activity with respect to a coupled simulation with CFB.

We furthermore test the parameterizations of the CFB based on wind-correction or stress-correction approaches as suggested by (Renault, Molemaker, McWilliams, et al., 2016) and (Renault, McWilliams, & Masson, 2017) and using an atmospheric forcing derived from a coupled simulation. These approaches are based on the use of a coupling coefficient between wind curl and current vorticity or stress curl and current vorticity. The coefficients can be estimated from a coupled simulation and prescribed to the forced oceanic simulation (c, i, and n in Figure 11) or predicted from the wind magnitude (b, f, and k in Figure 11). When forcing an oceanic simulation with a reanalysis product that does not account for the CFB, while both wind-correction and stress-correction approaches induce a slowdown of the mean circulation and a damping of the mesoscale activity, in contrast to a simulation forced with relative wind and without parameterization, they also allow representation of a partial re-energization of the mean oceanic circulation and of the mesoscale activity caused by the wind response (b and c in Figure 11). The best parameterization is the one based on a predicted s_τ (equation (10); b in Figure 11). Although all the parameterizations obtain relatively similar results in terms of mean and median EKE, the parameterization based on a predicted s_τ has the most realistic results with respect to the fully coupled simulation in eddy-rich regions such as Western Boundary Currents (b in Figure 11). Such a parameterization allows a simulation to represent more physics and to reproduce the daily and the spatial variability of s_τ, avoiding possible compensation of errors when using parameterizations based on prescribed coupling coefficients.

The parameterization based on a predicted s_τ has the advantage of flexibility because it can be used on top of a prescribed or estimated (with absolute wind) surface stress, thus allowing an oceanic model to be driven using climatological forcing. If the CFB effects are absent from both the wind and the stress of an atmospheric product, the user should take this parameterization using the α and β coefficients found in this study. If the CFB effects are present (as seems likely in future global reanalyses, labeled e–i in Figure 11), the surface currents should be known in a coherent way and filtered out (equations (11) or (12)) as using the parameterization based on the predicted s_τ (labeled f in Figure 11). In such a situation, one could use the α and β found in this study or estimate α and β using the surface currents, the surface stress, and the 10-m wind

from the atmospheric product. As shown in the supporting information, because of uncertainties related to the statistical procedure used to extract the mesoscale signal, the coefficients may be increased by ≈20%. This would have the effect of increasing the eddy killing by the α coefficient but also the re-energization by the β coefficient. However, even by using the coefficients obtained directly from the linear regression, the levels of EKE should be better represented than any other simulations based on the other parameterizations or, obviously, simulations without parameterizations of the CFB (e, g, and h in Figure 11).

Scatterometer products should not be treated as a reanalysis as scatterometer wind and stress already contain the CFB effects but in relation to an unknown current field. As a result, an uncoupled simulation forced by a scatterometer stress (or wind) product (j–n in Figure 11) may result in a realistic mean surface stress and give an accurate estimate of the mean oceanic circulation assuming that mean surface currents are mostly deterministic (with weak eddy-mean flow interactions) and are relatively well reproduced by a model (labels j and l in Figure 11). However, as in any simulation that uses prescribed surface stress without a parameterization of the CFB (or a wind without CFB), the eddies are not correctly damped because the estimated or the prescribed surface stress is not correlated with the simulated eddies. A mesoscale activity too intense may result in a too large an inverse cascade of energy, which might destabilize, for example, Western Boundary Currents (Renault, Marchesiello, et al., 2019). The use of a relative wind without a parameterization will lead, as for the case of a reanalysis, to a poor estimation of both the mean circulation and the mesoscale activity (m in Figure 11). An alternative is to use a scatterometer wind product with a bulk-formula stress and a parameterization of the wind response to avoid overestimation of the eddy damping (k and n in Figure 11). Because the 10-m wind product from a scatterometer represents the wind relative to the oceanic currents, using this wind with a bulk formula and a parameterization based on prescribed coupling coefficients (n in Figure 11) would, therefore, have a realistic eddy killing effect; however, the large-scale effect might be doubly accounted for, weakening the mean circulation. This has been recently shown to be important by Sun et al. (2019) for the North Equatorial Countercurrent. To overcome this issue, one could filter out the CFB imprint (as in f in 11) by using the parameterization based on a predicted s_τ and observed surface currents, for example, from AVISO (k in Figure 11). This should work if and only if the surface currents are known and are observed in a coherent way with the scatterometer wind and stress. However, the AVISO does not have the same effective resolution as QuikSCAT products and suffers from uncertainties. As a result, using the surface current from AVISO to correct, for example, QuikSCAT wind or stress does not allow reconstruction of clean wind or stress product.

Another topic related to this study deals with how to create a data set for forcing ocean models. As done by Large and Yeager (2009) and Tsujino et al. (2018), the time-mean wind speed from NCEP/NCAR and JRA55-do reanalysis, respectively, is adjusted to the time-mean QuikSCAT 10-m neutral relative wind. By doing so, these reanalyses may have the same issue as a scatterometer, that is, a double counting effect of the CFB on the large-scale circulation. To overcome this issue, one could simply add some time-mean ocean surface current to a scatterometer mean wind to estimate time-mean absolute wind using the coupling coefficients. However, again, the time-mean ocean surface current as estimated, for example, from AVISO does not have the same effective resolution as QuikSCAT products and suffers from uncertainties. As a result, adding the time-mean ocean surface current from AVISO to the QuikSCAT mean does not allow reconstruction of a clean time-mean absolute wind. Novels approaches, such as machine learning, could allow to identify oceanic features that imprint the stress by using various data set (such as SST, altimeters) and, thus, to filter out their imprint on scatterometer stress. Future satellite missions (such as SKIM; Ardhuin et al., 2017 and Chelton et al., 2018; Rodríguez et al., 2018; WaCM Bourassa et al., 2016) would likely allow measuring 10-m wind, surface stress, and surface currents in a consistent way and, thus, could be another option to construct a data set for forcing ocean models but also to estimate the α and β coefficients used to predict s_τ ((k) in Figure 11). They would help to better understand and characterize the wind and surface stress responses to both TFB and CFB.

In summary, forced oceanic models should take into account the CFB, which can be done by using the simple parameterizations tested in this study. These parameterizations should also be tested over ideal eddies and regional configurations to assess their effect on, for example, the eddy statistics and Western Boundary Currents dynamics, and we intend to investigate this soon. The wind response to the CFB can also alter the surface heat and freshwater fluxes, although, to our knowledge, this alteration has not been quantified precisely yet. On the one hand, a parameterization based on s_w not only allows us to compute the momentum flux response to the CFB but also heat and freshwater fluxes responses in a consistent way. On the other

hand, the parameterization based on a predicted s_τ allows a better representation of the mesoscale activity; however, it cannot represent the alteration of the surface heat and freshwater fluxes by the CFB. A possible solution to overcome this limitation is to combine the parameterization based on a predicted s_τ to estimate the surface stress with a parameterization based on s_w to take into account the surface heat and freshwater fluxes responses to the CFB. However, this approach does not guarantee that the same winds are used to compute the surface stress, turbulent heat fluxes, and evaporation as was done by Large and Yeager (2009). It therefore comes at the expense of decoupling turbulent heat and freshwater fluxes from the momentum flux. One question that arises from this study is then as follows: Should we favor a more realistic representation of mesoscale activity with an ad hoc approach (i.e., the parameterization based on s_τ) at the expense of a known relationship among the turbulent fluxes? It may also be noted that even when the wind speed is adjusted in a common manner, turbulent heat fluxes will differ greatly between model simulations, as heat fluxes depend strongly on SST, which is simulation dependent, via the heat-flux feedback (Large & Yeager, 2012). Moreover, in this study, the mesoscale TFB is not parameterized as we show that it does not have a strong impact on the mean and mesoscale circulations.

Acknowledgments
We appreciate the support from the National Science Foundation (OCE-1419450), from the California Natural Resources Agency (C0100400), and from the National Oceanic and Atmospheric Agency (NA15NOS4780186). This work was performed using HPC resources from GENCI-[CINES/IDRIS/TGCC] (Grants 2017-A0010106895, 2018-A0030106895, and 2019-A0050106895) and the Engineering Discovery Environment (XSEDE). T. A. and L. R. would like to thank HPC-Europa3 program, application HPC17IUTPN and HPC17MM0RX, respectively, and Barcelona Supercomputing Center (BSC) for hosting them. Data can be downloaded online (from http://research.atmos.ucla.edu/lrenault/HowTo/). The authors thank B. Barnier, E. Chassignet, G. Danabasoglu, F. Lemarié, K. Mogensen, J. Small, A.M. Treguier, and H. Tsujino for useful discussions. The authors want to thank three anonymous reviewers and J. Small for their careful and constructive comments.

References

Abel, R. (2018). Aspects of air-sea interaction in atmosphere-ocean models. Ph.D. thesis, Universität Kiel, Christian-Albrechts.

Ardhuin, F., Aksenov, Y., Benetazzo, A., Bertino, L., Brandt, P., Caubet, E., et al. (2017). Measuring currents, ice drift, and waves from space: the sea surface kinematics multiscale monitoring (skim) concept. *Ocean Science*. https://doi.org/10.5194/os-2017-65

Belmonte Rivas, M., & Stoffelen, A. (2019). Characterizing era-interim and era5 surface wind biases using ascat. *Ocean Science*, *15*(3), 831–852. https://doi.org/10.5194/os-15-831-2019

Bentamy, A., Grodsky, S. A., Chapron, B., & Carton, J. A. (2013). Compatibility of c-and ku-band scatterometer winds: Ers-2 and quikscat. *Journal of Marine Systems*, *117*, 72–80.

Betts, A., & Miller, M. (1986). A new convective adjustment scheme. part ii: Single column tests using gate wave, bomex, atex and arctic air-mass data sets. *Quarterly Journal of the Royal Meteorological Society*, *112*(473), 693–709.

Blanke, B., & Delecluse, P. (1993). Variability of the tropical atlantic ocean simulated by a general circulation model with two different mixed-layer physics. *Journal of Physical Oceanography*, *23*(7), 1363–1388. https://doi.org/10.1175/1520-0485(1993)023<1363:VOTTAO>2.0.CO;2

Bourassa, M. A., Rodriguez E., & Chelton D. (2016). Winds and currents mission: Ability to observe mesoscale air/sea coupling, In Geoscience and Remote Sensing Symposium (IGARSS), *2016 IEEE International* (pp. 7392–7395). IEEE.

Brodeau, L., Barnier, B., Gulev, S. K., & Woods, C. (2017). Climatologically significant effects of some approximations in the bulk parameterizations of turbulent air–sea fluxes. *Journal of Physical Oceanography*, *47*(1), 5–28. https://doi.org/10.1175/JPO-D-16-0169.1

Brodeau, L., Barnier, B., Treguier, A.-M., Penduff, T., & Gulev, S. (2010). An era40-based atmospheric forcing for global ocean circulation models. *Ocean Modelling*, *31*(3-4), 88–104. https://doi.org/10.1016/j.ocemod.2009.10.005

Bye, J. A. (1985). Large-scale momentum exchange in the coupled atmosphere-ocean. In J. Nihoul (Ed.), *Coupled ocean-atmosphere models, Elsevier oceanography series* (Vol. 40, pp. 51–61). Elsevier. https://doi.org/10.1016/S0422-9894(08)70702-5

Chassignet, E. P., & Marshall, D. P. (2013). Gulf stream separation in numerical ocean models. In M. W. Hecht & H. Hasumi (Eds.), *Ocean Modeling in an Eddying Regime*. Washington, DC: American Geophysical Union. https://doi.org/10.1029/177GM05.

Chelton, D. B., Esbensen, S. K., Schlax, M. G., Thum, N., Freilich, M. H., Wentz, F. J., et al. (2001). Observations of coupling between surface wind stress and sea surface temperature in the eastern tropical pacific. *Journal of Climate*, *14*(7), 1479–1498. https://doi.org/10.1175/1520-0442(2001)014<1479:OOCBSW>2.0.CO;2

Chelton, D. B., Schlax, M. G., Freilich, M. H., & Milliff, R. F. (2004). Satellite measurements reveal persistent small-scale features in ocean winds. *Science*, *303*(5660), 978–983. https://doi.org/10.1126/science.1091901

Chelton, D. B., Schlax, M. G., & Samelson, R. M. (2007). Summertime coupling between sea surface temperature and wind stress in the california current system. *Journal of Physical Oceanography*, *37*(3), 495–517. https://doi.org/10.1175/JPO3025.1

Chelton, D. B., Schlax, M. G., Samelson, R. M., Farrar, J. T., Molemaker, M. J., McWilliams, J. C., & Gula, J. (2018). Prospects for future satellite estimation of small-scale variability of ocean surface velocity and vorticity. *Progress in Oceanography*.

Chelton, D. B., & Xie, S.-P. (2010). Coupled ocean-atmosphere interaction at oceanic mesoscales. *Oceanography*, *23*(4), 52–69. https://doi.org/10.5670/oceanog.2010.05

Chen, F., & Dudhia, J. (2001). Coupling an advanced land surface–hydrology model with the penn state–ncar mm5 modeling system. part i: Model implementation and sensitivity. *Monthly Weather Review*, *129*(4), 569–585. https://doi.org/10.1175/1520-0493(2001)129<0569:CAALSH>2.0.CO;2

Chou, M.-D., & Suarez, M. J. (1999). A solar radiation parameterization (clirad-sw) for atmospheric studies. NASA Tech. Memo, *10460*, 48.

Colas, F., McWilliams, J. C., Capet, X., & Kurian, J. (2012). Heat balance and eddies in the peru-chile current system. *Climate Dynamics*, *39*(1-2), 509–529. https://doi.org/10.1007/s00382-011-1170-6

Cornillon, P., & Park, K. (2001). Warm core ring velocities inferred from NSCAT. *Geophysical Research Letters*, *28*(4), 575–578. https://doi.org/10.1029/2000GL011487

Craig, A., Valcke, S., & Coquart, L. (2017). Development and performance of a new version of the oasis coupler, oasis3-mct_3. 0. *Geoscientific Model Development*, *10*(9), 3297–3308. https://doi.org/10.5194/gmd-10-3297-2017

Dee, D., Uppala, S., Simmons, A., Berrisford, P., Poli, P., Kobayashi, S., et al. (2011). The era-interim reanalysis: Configuration and performance of the data assimilation system. *Quarterly Journal of the Royal Meteorological Society*, *137*(656), 553–597. https://doi.org/10.1002/qj.828

Desbiolles, F., Bentamy, A., Blanke, B., Roy, C., Mestas-Nuñez, A. M., Grodsky, S. A., et al. (2017). Two decades [1992-2012] of surface wind analyses based on satellite scatterometer observations. *Journal of Marine Systems*, *168*, 38–56. https://doi.org/10.1016/j.jmarsys.2017.01.003

Desbiolles, F., Blanke, B., Bentamy, A., & Roy, C. (2016). Response of the Southern Benguela upwelling system to fine-scale modifications of the coastal wind. *Journal of Marine Systems*, *156*, 46–55. https://doi.org/10.1016/j.jmarsys.2015.12.002

Dewar, W. K., & Flierl, G. R. (1987). Some effects of the wind on rings. *Journal of Physical Oceanography*, *17*(10), 1653–1667. https://doi.org/10.1175/1520-0485(1987)017<1653:SEOTWO>2.0.CO;2

Dong, C., McWilliams, J. C., Liu, Y., & Chen, D. (2014). Global heat and salt transports by eddy movement. *Nature Communications*, *5*(1), 3294. https://doi.org/10.1038/ncomms4294

Downes, S., Spence, P., & Hogg, A. (2018). Understanding variability of the southern ocean overturning circulation in core-ii models. *Ocean Modelling*, *123*, 98–109. https://doi.org/10.1016/j.ocemod.2018.01.005

Ducet, N., Le Traon, P.-Y., & Reverdin, G. (2000). Global high-resolution mapping of ocean circulation from TOPEX/Poseidon and ERS-1 and-2. *Journal of Geophysical Research*, *105*(C8), 19,477–19,498. https://doi.org/10.1029/2000JC900063

Duhaut, T. H., & Straub, D. N. (2006). Wind stress dependence on ocean surface velocity: Implications for mechanical energy input to ocean circulation. *Journal of Physical Oceanography*, *36*(2), 202–211. https://doi.org/10.1175/JPO2842.1

Fairall, C., Bradley, E. F., Hare, J., Grachev, A., & Edson, J. (2003). Bulk parameterization of air-sea fluxes: Updates and verification for the coare algorithm. *Journal of Climate*, *16*(4), 571–591. https://doi.org/10.1175/1520-0442(2003)016<0571:BPOASF>2.0.CO;2

Gaube, P., Chelton, D. B., Samelson, R. M., Schlax, M. G., & O'Neill, L. W. (2015). Satellite observations of mesoscale eddy-induced Ekman pumping. *Journal of Physical Oceanography*, *45*(1), 104–132. https://doi.org/10.1175/JPO-D-14-0032.1

Gruber, N., Lachkar, Z., Frenzel, H., Marchesiello, P., Münnich, M., McWilliams, J. C., et al. (2011). Eddy-induced reduction of biological production in Eastern Boundary Upwelling Systems. *Nature Geoscience*, *4*(11), 787–792. https://doi.org/10.1038/ngeo1273

Hallberg, R., & Gnanadesikan, A. (2006). The role of eddies in determining the structure and response of the wind-driven southern hemisphere overturning: Results from the modeling eddies in the southern ocean (meso) project. *Journal of Physical Oceanography*, *36*(12), 2232–2252. https://doi.org/10.1175/JPO2980.1

Hogg, A. M. C., Dewar, W. K., Berloff, P., Kravtsov, S., & Hutchinson, D. K. (2009). The effects of mesoscale ocean–atmosphere coupling on the large-scale ocean circulation. *Journal of Climate*, *22*(15), 4066–4082. https://doi.org/10.1175/2009JCLI2629.1

Hong, S.-Y., & Lim, J.-O. J. (2006). The wrf single-moment 6-class microphysics scheme (wsm6). *Journal of the Korean Meteorological Society*, *42*(2), 129–151.

Hong, S.-Y., Noh, Y., & Dudhia, J. (2006). A new vertical diffusion package with an explicit treatment of entrainment processes. *Monthly Weather Review*, *134*(9), 2318–2341. https://doi.org/10.1175/MWR3199.1

Janjić, Z. I. (1994). The step-mountain eta coordinate model: Further developments of the convection, viscous sublayer, and turbulence closure schemes. *Monthly Weather Review*, *122*(5), 927–945. https://doi.org/10.1175/1520-0493(1994)122<0927:TSMECM>2.0.CO;2

Jullien, S., Masson, M., Oerder, V., Samson, G., Colas, F., & Renault, L. (2020). Impact of ocean-atmosphere current feedback on the ocean mesoscale activity: regional variations, and sensitivity to model resolution. accepted in *Journal of Climate*. https://doi.org/10.1175/JCLI-D-19-0484.1

Kelly, K. A., Dickinson, S., McPhaden, M. J., & Johnson, G. C. (2001). Ocean currents evident in satellite wind data. *Geophysical Research Letters*, *28*(12), 2469–2472. https://doi.org/10.1029/2000GL012610

Large, W., & Yeager, S. (2012). On the observed trends and changes in global sea surface temperature and air–sea heat fluxes (1984–2006). *Journal of Climate*, *25*(18), 6123–6135. https://doi.org/10.1175/JCLI-D-11-00148.1

Large, W. G., & Yeager, S. (2009). The global climatology of an interannually varying air–sea flux data set. *Climate Dynamics*, *33*(2-3), 341–364. https://doi.org/10.1007/s00382-008-0441-3

Lemarié, F. (2015). Numerical modification of atmospheric models to include the feedback of oceanic currents on air-sea fluxes in ocean-atmosphere coupled models. Technical Report RT-464, INRIA Grenoble - Rhône-Alpes; Laboratoire Jean Kuntzmann; Universite de Grenoble I - Joseph Fourier; INRIA.

Luo, J.-J., Masson, S., Roeckner, E., Madec, G., & Yamagata, T. (2005). Reducing climatology bias in an ocean-atmosphere cgcm with improved coupling physics. *Journal of Climate*, *18*(13), 2344–2360. https://doi.org/10.1175/JCLI3404.1

Ma, X., Jing, Z., Chang, P., Liu, X., Montuoro, R., Small, R. J., et al. (2016). Western boundary currents regulated by interaction between ocean eddies and the atmosphere. *Nature*, *535*(7613), 533–537. https://doi.org/10.1038/nature18640

Madec, G. & NEMO-System-Team (2015). Nemo ocean engine. *Issue 27m* Scientific Notes of Climate Modelling Center.

Maronna, R. A., Martin, R. D., Yohai, V. J., & Salibián-Barrera, M. (2006). *Robust statistics: theory and methods (with R)*. John Wiley & Sons. https://doi.org/10.1002/0470010940

McGillicuddy, D. J., Anderson, L. A., Bates, N. R., Bibby, T., Buesseler, K. O., Carlson, C. A., et al. (2007). Eddy/wind interactions stimulate extraordinary mid-ocean plankton blooms. *Science*, *316*(5827), 1021–1026. https://doi.org/10.1126/science.1136256

McWilliams, J. C. (2008). The nature and consequences of oceanic eddies. *Ocean Modeling in an Eddying Regime*, 5–15. https://doi.org/10.1029/177GM03.

Minobe, S., Kuwano-Yoshida, A., Komori, N., Xie, S.-P., & Small, R. J. (2008). Influence of the Gulf Stream on the troposphere. *Nature*, *452*(7184), 206–209. https://doi.org/10.1038/nature06690

Mlawer, E. J., Taubman, S. J., Brown, P. D., Iacono, M. J., & Clough, S. A. (1997). Radiative transfer for inhomogeneous atmospheres: Rrtm, a validated correlated-k model for the longwave. *Journal of Geophysical Research*, *102*(D14), 16,663–16,682. https://doi.org/10.1029/97JD00237

Nakanishi, M., & Niino, H. (2006). An improved Mellor–Yamada level-3 model: Its numerical stability and application to a regional prediction of advection fog. *Boundary-Layer Meteorology*, *119*(2), 397–407. https://doi.org/10.1007/s10546-005-9030-8

O'Neill, L. W., Chelton, D. B., & Esbensen, S. K. (2003). Observations of sst-induced perturbations of the wind stress field over the southern ocean on seasonal timescales. *Journal of Climate*, *16*(14), 2340–2354. https://doi.org/10.1175/2780.1

O'Neill, L. W., Chelton, D. B., & Esbensen, S. K. (2010). The effects of sst-induced surface wind speed and direction gradients on midlatitude surface vorticity and divergence. *Journal of Climate*, *23*(2), 255–281. https://doi.org/10.1175/2009JCLI2613.1

O'Neill, L. W., Chelton, D. B., & Esbensen, S. K. (2012). Covariability of surface wind and stress responses to sea surface temperature fronts. *Journal of Climate*, *25*(17), 5916–5942. https://doi.org/10.1175/JCLI-D-11-00230.1

Oerder, V., Colas, F., Echevin, V., Masson, S., Hourdin, C., Jullien, S., et al. (2016). Mesoscale sst–wind stress coupling in the peru–chile current system: Which mechanisms drive its seasonal variability? *Climate Dynamics*, *47*(7-8), 2309–2330. https://doi.org/10.1007/s00382-015-2965-7

Oerder, V., Colas, F., Echevin, V., Masson, S., & Lemarié, F. (2018). Impacts of the mesoscale ocean-atmosphere coupling on the peru-chile ocean dynamics: The current-induced wind stress modulation. *Journal of Geophysical Research: Oceans*, *123*(2), 812–833. https://doi.org/10.1002/2017JC013294

Pacanowski, R. (1987). Effect of equatorial currents on surface stress. *Journal of Physical Oceanography*, *17*(6), 833–838. https://doi.org/10.1175/1520-0485(1987)017<0833:EOECOS>2.0.CO;2

Perlin, N., De Szoeke, S. P., Chelton, D. B., Samelson, R. M., Skyllingstad, E. D., & O'Neill, L. W. (2014). Modeling the atmospheric boundary layer wind response to mesoscale sea surface temperature perturbations. *Monthly Weather Review*, *142*(11), 4284–4307. https://doi.org/10.1175/MWR-D-13-00332.1

Plagge, A. M., Vandemark, D., & Chapron, B. (2012). Examining the impact of surface currents on satellite scatterometer and altimeter ocean winds. *Journal of Atmospheric and Oceanic Technology*, *29*(12), 1776–1793. https://doi.org/10.1175/JTECH-D-12-00017.1

Renault, L., Deutsch, C., McWilliams, J. C., Frenzel, H., Liang, J.-H., & Colas, F. (2016). Partial decoupling of primary productivity from upwelling in the california current system. *Nature Geoscience*, *9*(7), 505–508. https://doi.org/10.1038/ngeo2722

Renault, L., Lemarié, F., & Arsouze, T. (2019). On the implementation and consequences of the oceanic currents feedback in ocean-atmosphere coupled models. *Ocean Modelling*, *141*, 101423. https://doi.org/10.1016/j.ocemod.2019.101423

Renault, L., Marchesiello, P., Masson, S., & McWilliams, J. C. (2019). Remarkable control of western boundary currents by eddy killing, a mechanical air-sea coupling process. *Geophysical Research Letters*, *46*, 2743–2751. https://doi.org/10.1029/2018GL081211

Renault, L., Masson, S., Oerder, V., Jullien, S., & Colas, F. (2019). Disentangling the mesoscale ocean-atmosphere interactions. *Journal of Geophysical Research: Oceans*, *124*, 2164–2178. https://doi.org/10.1029/2018JC014628

Renault, L., McWilliams, J. C., & Masson, S. (2017). Satellite observations of imprint of oceanic current on wind stress by air-sea coupling. *Scientific Reports*, *7*(1), 17747. https://doi.org/10.1038/s41598-017-17939-1

Renault, L., McWilliams, J. C., & Penven, P. (2017). Modulation of the agulhas current retroflection and leakage by oceanic current interaction with the atmosphere in coupled simulations. *Journal of Physical Oceanography*, *47*(8), 2077–2100. https://doi.org/10.1175/JPO-D-16-0168.1

Renault, L., Molemaker, M. J., Gula, J., Masson, S., & McWilliams, J. C. (2016). Control and stabilization of the gulf stream by oceanic current interaction with the atmosphere. *Journal of Physical Oceanography*, *46*(11), 3439–3453. https://doi.org/10.1175/JPO-D-16-0115.1

Renault, L., Molemaker, M. J., McWilliams, J. C., Shchepetkin, A. F., Lemarié, F., Chelton, D., et al. (2016). Modulation of wind work by oceanic current interaction with the atmosphere. *Journal of Physical Oceanography*, *46*(6), 1685–1704. https://doi.org/10.1175/JPO-D-15-0232.1

Rodríguez, E., Wineteer, A., Perkovic-Martin, D., Gál, T., Stiles, B. W., Niamsuwan, N., & Monje, R. R. (2018). Estimating ocean vector winds and currents using a ka-band pencil-beam doppler scatterometer. *Remote Sensing*, *10*(4), 576. https://doi.org/10.3390/rs10040576

Rooth, C., & Xie, L. (1992). Air-sea boundary layer dynamics in the presence of mesoscale surface currents. *Journal of Geophysical Research, Oceans*, *97*(C9), 14,431–14,438. https://doi.org/10.1029/92JC01296

Saha, S., Moorthi, S., Pan, H.-L., Wu, X., Wang, J., Nadiga, S., et al. (2010). The NCEP climate forecast system reanalysis. *Bulletin of the American Meteorological Society*, *91*(8), 1015–1058. https://doi.org/10.1175/2010BAMS3001.1

Samson, G., Masson, S., Durand, F., Terray, P., Berthet, S., & Jullien, S. (2017). Roles of land surface albedo and horizontal resolution on the indian summer monsoon biases in a coupled ocean–atmosphere tropical-channel model. *Climate Dynamics*, *48*(5-6), 1571–1594. https://doi.org/10.1007/s00382-016-3161-0

Scott, R. B., & Xu, Y. (2009). An update on the wind power input to the surface geostrophic flow of the world ocean. *Deep Sea Research Part I: Oceanographic Research Papers*, *56*(3), 295–304. https://doi.org/10.1016/j.dsr.2008.09.010

Seo, H. (2017). Distinct influence of air–sea interactions mediated by mesoscale sea surface temperature and surface current in the arabian sea. *Journal of Climate*, *30*(20), 8061–8080. https://doi.org/10.1175/JCLI-D-16-0834.1

Seo, H., Miller, A. J., & Norris, J. R. (2016). Eddy–wind interaction in the california current system: Dynamics and impacts. *Journal of Physical Oceanography*, *46*(2), 439–459. https://doi.org/10.1175/JPO-D-15-0086.1

Seo, H., Subramanian, A. C., Song, H., & Chowdary, J. S. (2019). Coupled effects of ocean current on wind stress in the bay of bengal: Eddy energetics and upper ocean stratification. *Deep Sea Research Part II: Topical Studies in Oceanography*, *168*, 104617. https://doi.org/10.1016/j.dsr2.2019.07.005

Shchepetkin, A. F., & McWilliams, J. C. (2009). Correction and commentary for "ocean forecasting in terrain-following coordinates: Formulation and skill assessment of the regional ocean modeling system" by haidvogel et al., j. comp. phys. 227, pp. 3595–3624. *Journal of Computational Physics*, *228*(24), 8985–9000. https://doi.org/10.1016/j.jcp.2009.09.002

Shin, H. H., Hong, S.-Y., & Dudhia, J. (2012). Impacts of the lowest model level height on the performance of planetary boundary layer parameterizations. *Monthly Weather Review*, *140*(2), 664–682. https://doi.org/10.1175/MWR-D-11-00027.1

Skamarock, W. C., Klemp, J. B., Dudhia, J., Gill, D. O., & Barker, D. (2008). *A description of the advanced research WRF version 3* (NCAR Technical Report No. NCAR/TN-475STR). Boulder, CO: National Center for Atmospheric Research.

Small, R., Xie, S., O'Neill, L., Seo, H., Song, Q., Cornillon, P., et al. (2008). Air–sea interaction over ocean fronts and eddies. *Dynamics of Atmospheres and Oceans*, *45*(3-4), 274–319. https://doi.org/10.1016/j.dynatmoce.2008.01.001

Small, R. J., Richards, K. J., Xie, S.-P., Dutrieux, P., & Miyama, T. (2009). Damping of tropical instability waves caused by the action of surface currents on stress. *Journal of Geophysical Research, Oceans*, *114*, C04009. https://doi.org/10.1029/2008JC005147

Song, Q., Chelton, D. B., Esbensen, S. K., Thum, N., & O'Neill, L. W. (2009). Coupling between sea surface temperature and low-level winds in mesoscale numerical models. *Journal of Climate*, *22*(1), 146–164. https://doi.org/10.1175/2008JCLI2488.1

Sun, Z., Liu, H., Lin, P., Tseng, Y.-h., Small, J., & Bryan, F. (2019). The modeling of the north equatorial countercurrent in the community earth system model and its oceanic component. *Journal of Advances in Modeling Earth Systems*, *11*, 531–544. https://doi.org/10.1029/2018MS001521

Tsujino, H., Urakawa, S., Nakano, H., Small, R. J., Kim, W. M., Yeager, S. G., et al. (2018). Jra-55 based surface dataset for driving ocean–sea-ice models (jra55-do). *Ocean Modelling*, *130*, 79–139. https://doi.org/10.1016/j.ocemod.2018.07.002

Xu, Y., & Scott, R. B. (2008). Subtleties in forcing eddy resolving ocean models with satellite wind data. *Ocean Modelling*, *20*(3), 240–251. https://doi.org/10.1016/j.ocemod.2007.09.003